X-551-69-434
PREPRINT

NASA TM X- 63787

NASA MINITRACK INTERFEROMETER REFRACTION CORRECTIONS

P. E. SCHMID

OCTOBER 1969

GSFC
GODDARD SPACE FLIGHT CENTER
GREENBELT, MARYLAND

X-551-69-434
PREPRINT

NASA MINITRACK INTERFEROMETER

REFRACTION CORRECTIONS

P. E. Schmid

October 1969

Goddard Space Flight Center
Greenbelt, Maryland

PRECEDING PAGE BLANK NOT FILMED.

CONTENTS

CONTENTS

NASA MINITRACK INTERFEROMETER REFRACTION CORRECTIONS

P. E. Schmid

ABSTRACT

The NASA Minitrack interferometer system is an accurate, reliable and proven spacecraft tracking system. This report reviews the influence of the Earth's atmosphere upon Minitrack calibration and spacecraft tracking. It is believed that this review will aid the orbit computation engineer in selecting those refraction correction procedures which will assure maximum orbit computation accuracy whenever an interferometer such as the Minitrack system is employed.

NASA MINITRACK INTERFEROMETER REFRACTION CORRECTIONS

P. E. Schmid

SUMMARY

This report examines the refraction effects of the Earth's atmosphere on the NASA 136 MHz Minitrack interferometer during aircraft calibration and spacecraft tracking. It is shown that only the troposphere (sea level to 30 km) affects aircraft calibration. It is also seen that the ionosphere (85 km to 1000 km above Earth's surface) is the principal refraction bias source during spacecraft track. This results from the troposphere correction inherent in an interferometer angle calculation.

The daytime ionosphere induced bias at 25° elevation can be as large as 1 mr. This bias decreases to 0.1 mr at 80° elevation. Nighttime, when total ionosphere electron content decreases, generally results in only 10% of the daytime refraction. Possible exceptions have been cited for near equatorial stations where nighttime anomolous ionospheric behavior has caused Minitrack signal dropouts of telemetry and tracking data. This anomaly when present has been noted to generally peak at local midnight. It is clear that ionospheric refraction corrections are a necessary part of Minitrack data processing if daytime data below elevation angles of 45° is to be used for precision orbit computation. This is required to reduce the ionospheric refraction bias to a value comparable to the Minitrack system resolution of 0.1 mr.

NASA MINITRACK INTERFEROMETER REFRACTION CORRECTIONS

1.0 INTRODUCTION

This report reviews the influence of the Earth's atmosphere upon NASA Minitrack measurements during system calibration and spacecraft tracking. The need for such a review stems from the increased number of precision orbits now being generated based upon Minitrack data (for example Reference 1), coupled with a lack of formal documentation in the area of Minitrack refraction modeling. The basic considerations presented in this report apply equally well to any short baseline radio interferometer tracking system.

Section 2.0 of this report briefly compares the angle information provided by an interferometer such as Minitrack with that obtained from steerable antenna systems. NASA steerable or monopulse tracking systems include;

1. The Goddard Range and Range Rate System (Reference 2)

2. The Unified S-Band System (Reference 3)

3. Pulse C-Band radar (Reference 4)

4. and the Applications Technology Satellite Range and Range Rate System (Reference 5)

The Earth's atmosphere can for purposes of radiowave propagation analysis be considered to consist of three layers. These layers, as indicated by Figure 1, are a function of altitude above the earth's surface and include the:

1. Troposphere $0 < h < 30$ km

2. Free-space Region $30 < h < 85$ km

3. Ionosphere $85 < h < 1000$ km

Section 3.0 presents a brief description of the frequency independent tropospheric angle correction equations appropriate to steerable antenna spacecraft tracking. Section 4.0 then indicates why the interferometer, to a first order, inherently corrects for tropospheric refraction when the baseline length is measured in free space wavelengths at the spacecraft transmitter frequency. In Section 5

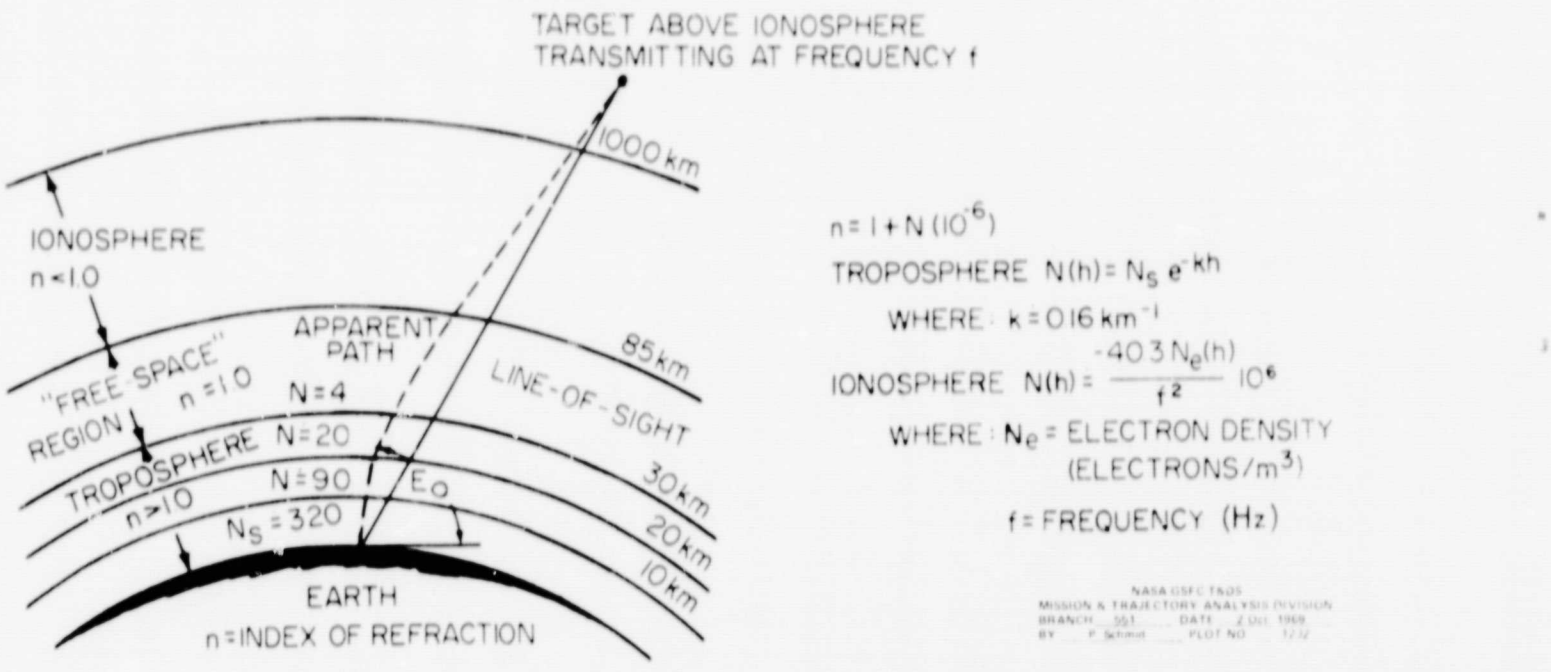

Figure 1–Relationship Between Troposphere and Ionosphere

it is shown that the effect of the one way Doppler shift upon Minitrack measurement does not significantly detract from this tropospheric angle correction.

Section 5.0 of this report reviews the philosophy of the present Minitrack aircraft calibration procedure indicating the significance of radio and optical refraction. Equations are derived which properly model the atmosphere for purposes of calibration computations. These particular equations are incorporated in the Minitrack star background photo plate reduction computer program used by the Physical Science Laboratory, New Mexico State University for the Goddard Space Flight Center.

Finally, section 6.0, indicates what improvements can be anticipated by modeling the ionosphere. Ionospheric ray bending decreases in proportion to the square of transmission frequency (Reference 6). Thus the distortion introduced by the ionosphere with an interferometer operating at S-Band frequencies (nominal 2 GHz) is reduced by a factor of approximately 200 relative to that at 136 MHz. By contrast, the tropospheric bending is frequency independent in the frequency range of 100 MHz to 20 GHz (Reference 7).

Figure 2 indicates the overall Minitrack data handling and aircraft calibration interface. With regard to Figure 2, this report is primarily concerned with

1. the optical and radio refraction corrections applied to the aircraft calibration data and,

2. the inherent troposphere corrections associated with data delivered to the orbit computation user and ionospheric refraction during spacecraft tracking.

Currently aircraft calibration flights are performed approximately twice per year for each of the NASA Minitrack stations. The site locations are presented in Figure 3. The Minitrack and the Goddard Range and Range Rate systems are the primary tracking systems associated with the NASA Satellite tracking and Data Acquisition Network (STADAN).

It should be mentioned that the primary purpose of the aircraft calibration is to determine the far-field phase characteristics of the Minitrack antenna array. The possibility of obtaining the same information via residual analysis from actual Minitrack satellite orbit calculations is currently under investigation (Reference 9). A regression analysis of this type appears feasible if multiple station, short arc passes are considered. Uncertainties in the earth geopotential function tend to mask tracking system biases when more than one earth revolution is calculated (Reference 10).

2.0 INTERFEROMETER VERSUS STEERABLE ANTENNA ANGLE MEASUREMENT

The Minitrack system is an interferometer tracking scheme (References 11 and 12) which provides angular data in the form of direction cosines describing the position of a spacecraft relative to a given tracking station. It is a passive system where the spacecraft transmits at a nominal 136 MHz. Hence no ranging information is available and at present no attempt is made to utilize the available one way Doppler frequency information for range rate calculations. The relationships between direction cosines and the conventional definitions of azimuth and elevation are given in Figure 4. As will be shown, the Minitrack direction cosine calculation does not provide a measure of either signal elevation angle of arrival or line-of-sight elevation to spacecraft but rather an elevation angle between the two which to a first order is the angle of arrival corrected for tropospheric refraction. Elevation angle of arrival is the elevation angle of the incoming, essentially planar, wavefront. Line-of-sight elevation is with reference to the straight line segment joining the interferometer array center and the spacecraft.

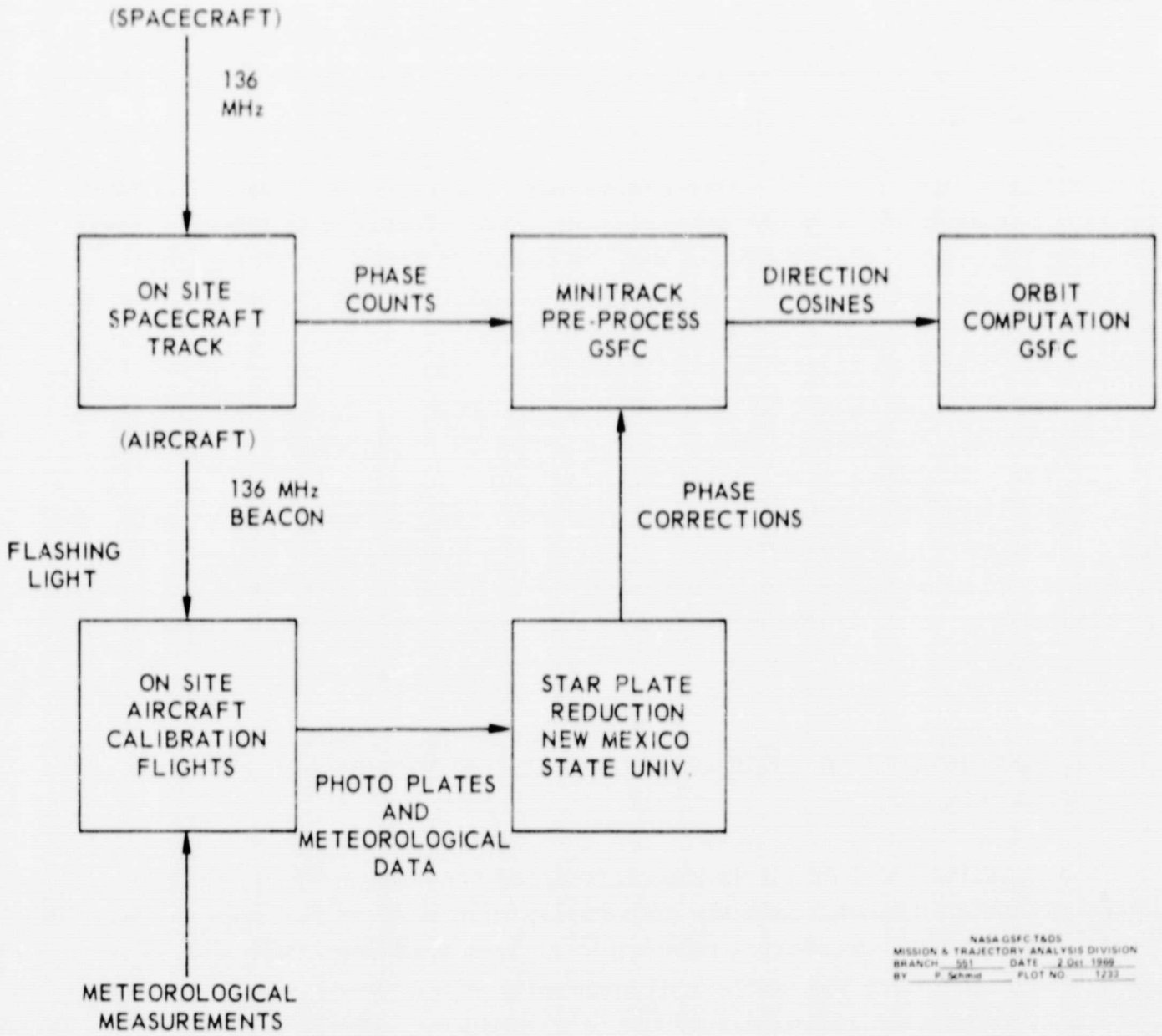

NASA GSFC T&DS
MISSION & TRAJECTORY ANALYSIS DIVISION
BRANCH 551 DATE 2 Oct. 1969
BY P. Schmid PLOT NO. 1233

Figure 2–Overall Minitrack Data Handling

This is in contrast to the elevation angle of arrival measure provided by tracking systems employing steerable antennas (e.g., the NASA Unified S-Band,

Station	Latitude			Longitude			Geodetic Height
	(deg.	min.	sec.)	(deg.	min.	sec.)	(meters)
Fairbanks, Alaska	64	52	18.61	212	09	40.15	189
Goldstone Lake, California	35	19	48.56	243	06	00.85	921
East Grand Forks, Minnesota	48	01	21.18	262	59	21.05	249
Fort Myers, Florida	26	32	53.78	278	08	04.60	9
Blossom Point, Maryland	38	25	49.91	282	54	49.37	6
St. John's, Newfoundland	47	44	28.94	307	16	46.71	112
Quito, Ecuador	-00	37	20.55	281	25	15.62	3578
Lima, Peru	-11	46	34.86	282	50	59.14	34
Antofagasta, Chile	-23	37	14.07	289	43	38.32	516
Santiago, Chile	-33	08	56.23	289	19	52.88	681
Winkfield, England	51	26	45.43	359	18	13.57	37
Johannesburg, South Africa	-25	53	00.98	27	42	28.49	1565
Tananarive, Madagascar	-19	00	25.21	47	18	00.46	1361

(Reference 8)

Note: Not all of the indicated sites are currently active (Oct. 1969).

Geodetic Positions on MERCURY Datum

a = 6 378 166m — equatorial radius

1/f = 298.3 — flattening factor

where:

$$f = \frac{a - b}{a}$$

b = polar radius of earth ellipsoid

Figure 3–Satellite Tracking and Data Acquisition Network (STADAN) Minitrack Stations

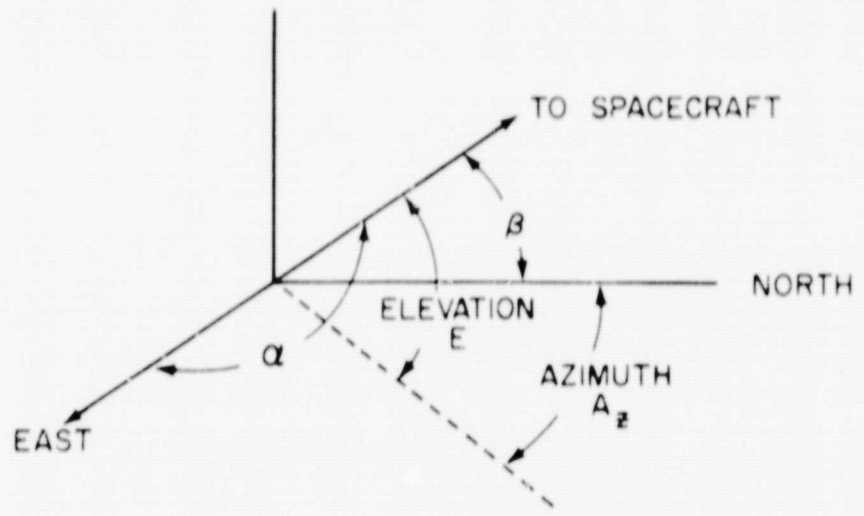

$$\cos E = (\ell^2 + m^2)^{1/2} \qquad \ell \equiv \cos\alpha = \text{SIN AZ COS E}$$

$$\cos AZ = \frac{m}{(\ell^2 + m^2)^{1/2}} \qquad m \equiv \cos\beta = \text{COS AZ COS E}$$

Figure 4–Definition of Minitrack Coordinate System

Goddard Range and Range Rate, and Pulse C-Band radar systems). The elevation angle of arrival is of course available directly from an azimuth-elevation antenna mount.

It can be obtained by way of straight forward coordinate transformations when the angle data is measured with X-Y or polar antenna mounts (Reference 13).

3.0 TROPOSPHERIC ANGLE CORRECTION APPLIED TO STEERABLE ANTENNA TRACKING SYSTEMS

The usual correction scheme applied to elevation angle data obtained from tracking systems employing steerable antennas is:

$$E = E_0 - \Delta E = E_0 - \Delta E_t - \Delta E_i \qquad (1)$$

E_0 = observed elevation angle of arrival

ΔE = a correction accounting for atmospheric bending

ΔE_t is associated with tropospheric bending

ΔE_i is associated with ionospheric bending

It should be pointed out that the effect of the ionosphere's presence is always to increase the error angle ΔE above that due to the troposphere alone. Since the bending within the ionosphere is in a direction opposite to that within the troposphere, one might guess that the effects are partially compensating. That this is not the case, will be shown in section 6.0. However, an intuitive answer can be obtained with reference to Figure 5. By considering a fixed angle of arrival, E_0 , one can observe what the error, ΔE, will be for various spacecraft altitudes.

For a given angle of arrival, the ray path is determined and hence the line-of-sight angle E will always be between the tracking station and a point on the ray trace corresponding to the spacecraft altitude, h . As is suggested by Figure 5, the error angle ($\Delta E = E_0 - E$) will never be less than the error due to the troposphere alone. The error actually has a maximum when the spacecraft is within the ionosphere and tends to that due to the troposphere alone as the spacecraft altitude reaches an altitude of several thousand kilometers above the earth's surface.

The correction represented by ΔE_t (equation 1) is frequency independent in the range 100 to 20000 MHz. The correction represented by ΔE_i (equation 1) varies inversely as the square of frequency. At frequencies greater than 1 GHz and at elevations greater than 5° the ionosphere accounts for no more than 2% of the total refraction (Reference 6). At 136 MHz, however, the tropospheric and ionospheric refraction effects can be comparable depending upon spacecraft altitude. The tropospheric first order elevation correction for tracking spacecraft at altitudes greater than 100 km and $E_0 > 10°$ with a steerable antenna is given by: (References 14, 15, 16).

$$\Delta E_t = N_s (10^{-6}) \cot E_0 \text{ radians} \qquad (2)$$

where: ΔE_t and E_0 are as defined previously and N_s , the surface refractivity, is a convenient measure of surface index of refraction.

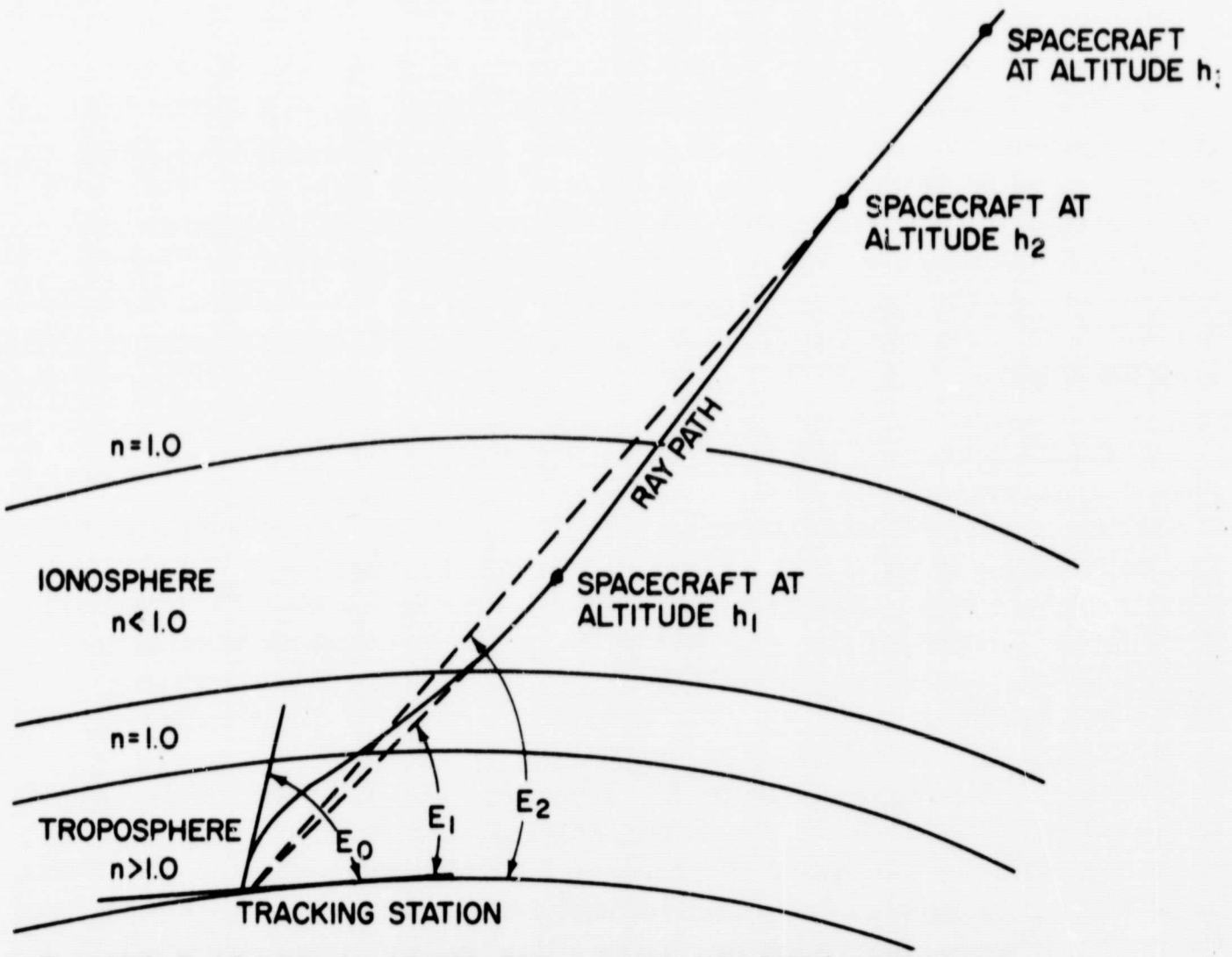

E_0 = ANGLE OF ARRIVAL (FIXED FOR A GIVEN RAY PATH) = CONSTANT
E = LINE-OF-SIGHT ELEVATION (i.e. E_1 AND E_2 RESPECTIVELY)
ERROR ANGLE $\equiv \Delta E = E_0 - E$
NOTE THAT $\Delta E_1 > \Delta E_2$ AND $\Delta E \rightarrow$ CONSTANT AS $h \rightarrow \infty$

NASA GSFC T&DS
MISSION & TRAJECTORY ANALYSIS DIVIS
BRANCH 551 DATE 2 Oct 1969
BY P. Schmid PLOT NO 1235

Figure 5–Increase in Elevation Angle Error Due to Ionosphere

$$n_s = 1 + N_s\ (10^{-6}) \tag{3}$$

The surface refractivity, N_s, can be computed from:

$$N = \frac{77.6}{T}\left(P + \frac{4810\ e_s\ RH}{T}\right) \tag{4}$$

where:

T = temperature in degrees Kelvin

P = total atmospheric pressure (millibars)

RH = relative humidity

e_s = saturation vapor pressure (millibars)

Equations (1) and (2) can also be written in terms of direction cosines. For frequencies above 1 GHz the ionospheric contribution to ray bending is usually considered negligible and equation (1) becomes:

$$E = E_0 - N_s\ (10^{-6})\ \cot E_0 \tag{5}$$

or

$$\cos E = \cos\ [E_0 - (10^{-6})\ N_s\ \cot E_0] = \cos E_0\ [1 + N_s\ (10^{-6})] \tag{6}$$

since $N_s\ (10^{-6})\ \cot E_0 \ll E_0$ for $E_0 > 5^0$

but from Figure 4

$$\ell = \cos \alpha = \sin AZ \cos E$$

$$m = \cos \beta = \cos AZ \cos E$$

and letting ℓ_0, m_0 represent angle of arrival direction cosines with ℓ, m representing "best estimate" of line-of-sight direction cosines, it is seen that:

$$\ell = [1 + N_s (10^{-6})] \ \ell_0 \tag{7}$$

and

$$m = [1 + N_s (10^{-6})] \ m_0 \tag{8}$$

Summarizing then, it is seen that a steerable antenna (i.e. monopulse) tracking system when corrected for first order tropospheric bending effects, results in the angle of arrival direction cosine adjustments indicated by equations (7) and (8). The next section will show that this tropospheric correction is inherent in the Minitrack direction cosine calculation.

4.0 TROPOSPHERIC ANGLE CORRECTION INHERENT IN INTERFEROMETER MEASUREMENTS

An ideal radio interferometer measurement will be defined as one where the incident signal is planar and operation is within a stabile (i.e. time invariant over measurement period) spherically stratified exponential troposphere. These conditions are for all practical purposes met when radio energy is received from a spacecraft at altitudes in excess of 100 km above the Earth's surface and when frequencies in excess of 1 GHz are employed thus obviating consideration of the ionosphere. At lower frequencies such as the 136 MHz transmission of Minitrack signals, the ionosphere will also affect the angle measurement. However, this ionospheric effect can be shown to produce a linear addition to elevation angle measurement which will appear as a residual error once the troposphere has been taken into account. The following derivation shows that the ideal interferometer provides a "built in" first order correction for the tropospheric effect and that this correction is the same as is normally applied to elevation angle data obtained from steerable antenna trackers (i.e. equation 2).

4.1 THE BASIC MINITRACK MEASUREMENT

As suggested by Figure 6, the basic measurement of an orthogonally intersecting interferometer such as Minitrack, are the direction cosines ℓ and m. More precisely, however, the measurement is a phase comparison, which

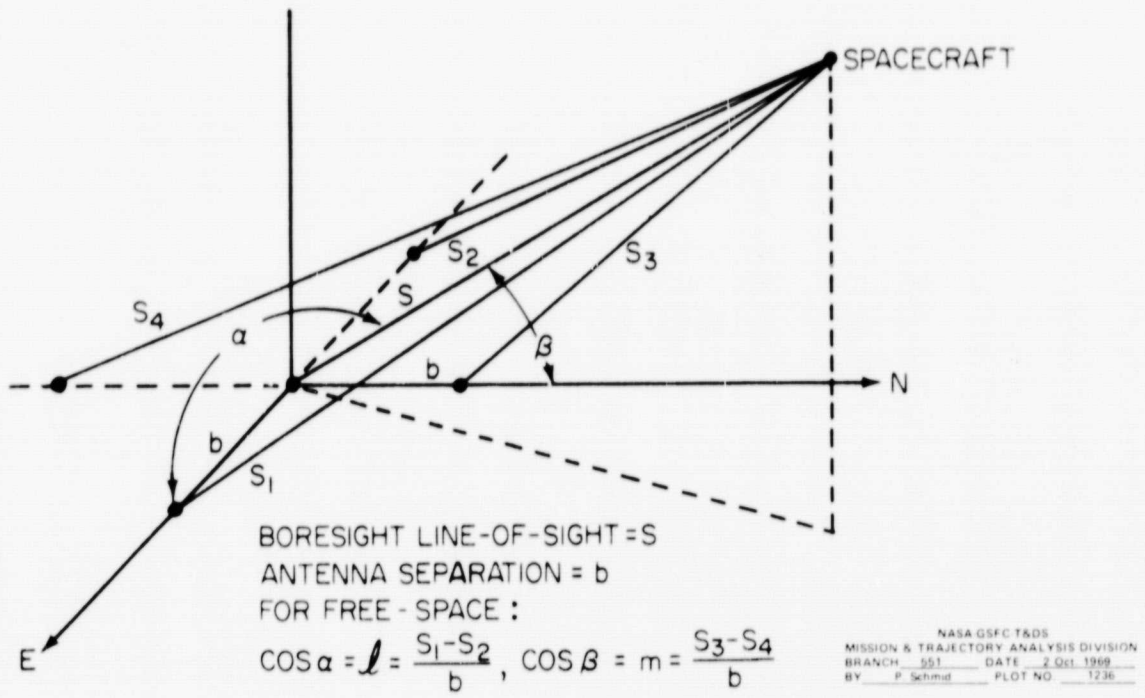

Figure 6–Simplified Diagram of Minitrack Interferometer Spacecraft Tracking

for each antenna pair, provides a measure of radio path length difference. This is indicated in figure 6 where $\triangle S_1$ and $\triangle S_2$ in actual operation represent radio path length differences rather than geometric differences associated with operation within free space. The object of all elevation angle corrections to radio tracking data is to approximate the geometric line of sight elevation angle between tracking stations and spacecraft as closely as possible. This line of sight is indicated by S of Figure 6.

The phase measurement associated with the two interferometer antenna pairs is indicated in Figure 7.

With reference to Figure 6, the direction cosines ℓ_0 , m_0 of the angle of arrival are given by:

$$\ell_0 = \cos\alpha_0 = \frac{M_1 \lambda_s}{b} \tag{9}$$

$$m_0 = \cos\beta_0 = \frac{M_2 \lambda_s}{b} \tag{10}$$

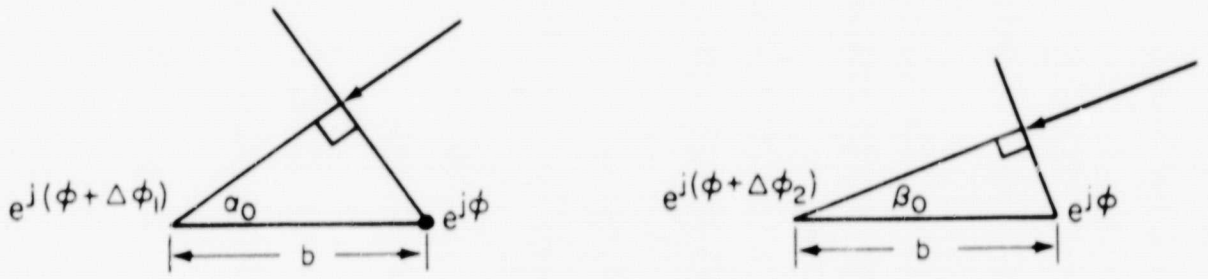

WHERE α_0 AND β_0 ARE RESPECTIVE INTERFEROMETER ANGLES CORRESPONDING TO THE WAVEFRONT ANGLE OF ARRIVAL, E_0

NASA GSFC T&DS
MISSION & TRAJECTORY ANALYSIS DIVISION
BRANCH 551 DATE 2 Oct 1969
BY P. Schmid PLOT NO 1237

Figure 7–Interferometer Phase Measurement

where M_1 and M_2 are respective whole and fractional cycles of phase shift measured by the Minitrack system, λ_s, is the signal wavelength as measured in the refractive media in the immediate vicinity of the interferometer, and b is the baseline separation of each of the interferometer legs.

4.2 MINITRACK ANGLE COMPUTATION

The information contained in the raw tracking data is M_1 and M_2 to some ambiguity. At Goddard ambiguities are resolved and the phase counts are converted to direction cosines using baseline separation in free space wavelengths, λ_0, rather than the actual wavelength indicated in equations 9 and 10 (reference 30). Thus the angles α', β' calculated using free space baseline separation are not a measure of angle of arrival but some "pseudo angle" which is linked to the angle of arrival by the surface index of refraction. That is:

$$\lambda_s = \frac{\lambda_0}{n_s} \tag{11}$$

and hence

$$\cos \alpha' = \ell' = n_s \cos \alpha_0 = [1 + N_s (10^{-6})] \ell_0 \qquad (12)$$

similarly

$$m' = [1 + N_s (10^{-6})] m_0 \qquad (13)$$

where ℓ' and m' are calculated direction cosines, and ℓ_0 and m_0 are angle of arrival direction cosines. However, equations 12 and 13 are seen to be exactly the results presented previously by equations 7 and 8 where a first order tropospheric correction had been applied to a monopulse (steerable antenna) tracking system. Thus the Minitrack angle calculation has a "built in" tropospheric refraction correction which for $E_0 > 10°$ accounts for at least 98% of the tropospheric bending. If no atmospheric corrections are applied to Minitrack data it can be expected that the primary refraction effect of the Earth's atmosphere will be linked to the ionosphere.

5.0 OPTICAL AND RADIO REFRACTION DURING MINITRACK CALIBRATION

At present the Minitrack system is calibrated by means of aircraft which carry both optical and radio beacons. The optical beacon is photographed against a star background which permits a precise means for determining the line of sight between station and aircraft (References 17 and 18).

The primary purpose of the aircraft flyby is to determine the far field phase characteristics of the Minitrack antenna array. Since Minitrack antenna spacing corresponding to each of the intersecting baselines is on the order of 50 wavelengths, the far field should be probed at slant ranges of approximately 10 km or greater. The aircraft also provides a "zero set" phase measurement which accounts for inequalities in cable electrical length between respective antenna arrays and the Minitrack receiver. These cables are filled with moisture free Nitrogen and maintained at an approximate gauge pressure of 5 pounds per square inch. In addition to the aircraft flyby, internal Minitrack system calibrations are performed to account for electronic equipment phase delays.

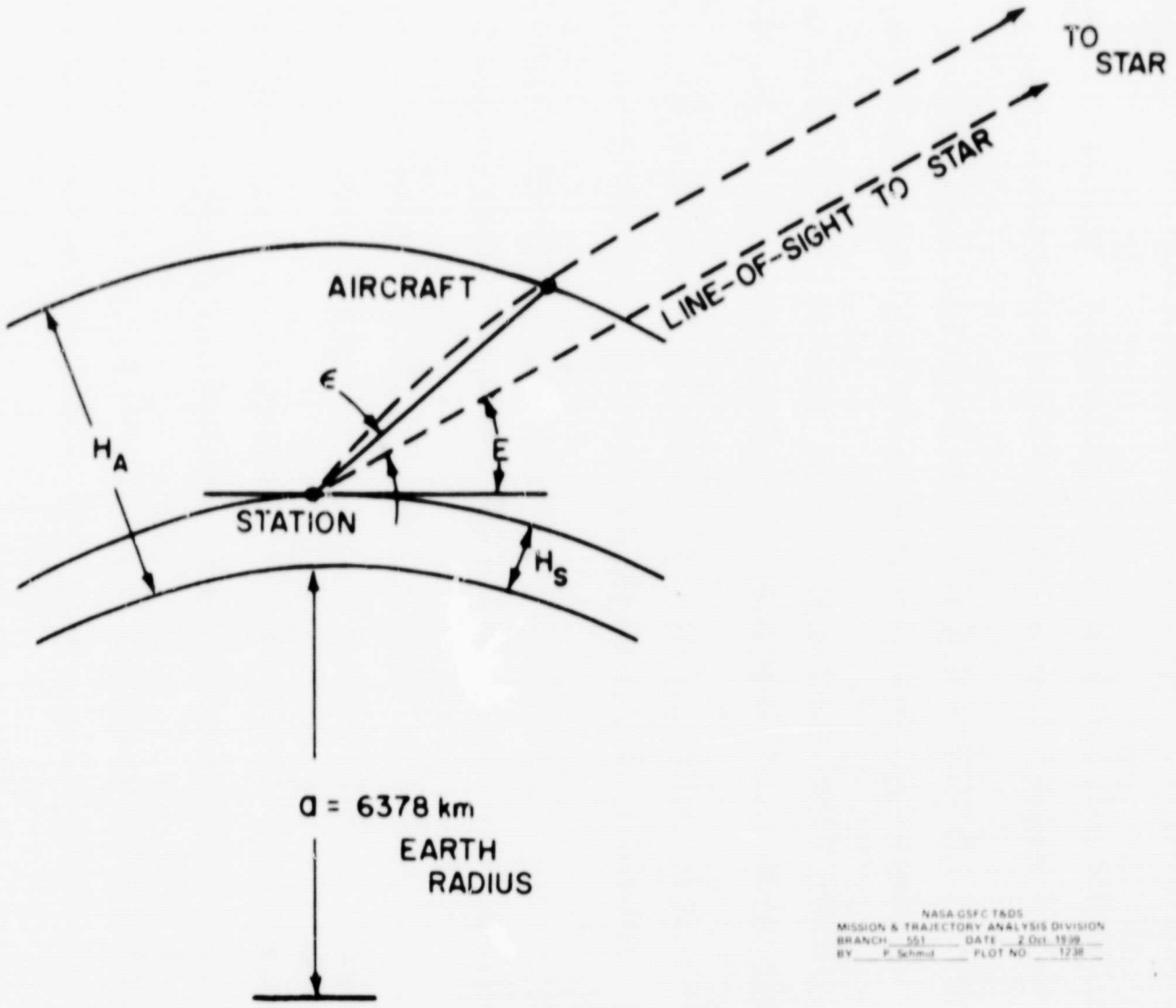

NASA GSFC T&DS
MISSION & TRAJECTORY ANALYSIS DIVISION
BRANCH 551 DATE 2 Oct. 1969
BY P. Schmid PLOT NO. 1238

Figure 8–Optical Refraction Geometry

5.1 CALIBRATION AND OPTICAL REFRACTION

As indicated in Figure 8, the calibration aircraft is photographed against a star background. The line-of-sight from the center of the Minitrack orthogonal pair of interferometers to a given star is then accurately determined since the star field has been well established by astronomers. However, the line of sight to the aircraft is different than the line-of-sight to the star by a small angle ϵ. This angle, ϵ, must be added to the line-of-sight angle to the star to provide an optical line-of-sight to the aircraft which is then corrected for radio refraction to permit a calculation of what the interferometer should read at 136 MHz. An expression for the angle, ϵ, has been rigorously derived in Reference 19.

As will be shown in section 6.0 it is also given to a good approximation by:

$$\epsilon = \left(n_0 - 2 + \frac{\bar{n}}{n_0} \right) \cot E \quad \text{(radians)} \tag{14}$$

where:

E = elevation angle to the star

$\bar{n}$ = average optical index of refraction between Minitrack station and aircraft altitudes

$$= \frac{1}{H_A - H_s} \int_{H_s}^{H_A} n(h)\, dh$$

n_0 = surface optical index of refraction

H_A = altitude of aircraft above sea level

H_s = altitude of tracking station above sea level

which for an exponential spherically stratified troposphere (i.e. $n(h) = 1 + N_0(10^{-6})\, e^{-\gamma h}$) leads to:

$$\epsilon \doteq \frac{N_0(10^{-6}) \cot E \left[1 - e^{-\gamma(H_A - H_s)}\right]}{\gamma(H_A - H_s)} \text{ (radians)} \qquad (15)$$

The validity of the exponential model for purposes of radio refraction correction has been well established (Reference 20, 14, 7).

With regard to equation (15) the optical surface refractivity N_0 can be calculated from:

$$N_0 = \frac{77.6\, p}{T} \qquad (16)$$

where

p = total atmospheric pressure (mb)

T = air temperature (°K) and

The decay constant, γ, for the optical index of refraction within the Earth's atmosphere is approximately 0.1 km^{-1} (Reference 19).

The next step is to determine what the Minitrack direction cosine measurements should be, based upon the line-of-sight angle to the aircraft ($E + \epsilon$ of Figure 8). Let $\cos \alpha$, $\cos \beta$ be the direction cosines to the star coincident with the flashing light and $\cos \alpha'$, $\cos \beta'$ be the desired line-of-sight direction cosines to the aircraft. Then:

$$\cos \alpha' = \cos \alpha \left(\frac{\cos \alpha'}{\cos \alpha} \right) \tag{17}$$

and

$$\cos \beta' = \cos \beta \left(\frac{\cos \beta'}{\cos \beta} \right) \tag{18}$$

from previous definitions

$$\cos \alpha = \sin AZ \cos E$$

$$\cos \beta = \cos AZ \cos E$$

$$\cos \alpha' = \sin AZ \cos (E + \epsilon) \doteq \sin AZ (\cos E - \epsilon \sin E) \tag{19}$$

$$\cos \beta' = \cos AZ \cos (E + \epsilon) \doteq \cos AZ (\cos E - \epsilon \sin E) \tag{20}$$

Thus the ratios $\cos \alpha' / \cos \alpha$ and $\cos \beta' / \cos \beta$ (equations 17 and 18 respectively) are given by:

$$\frac{\cos \alpha'}{\cos \alpha} = \frac{\cos \beta'}{\cos \beta} = 1 - \epsilon \tan E = (1 - K) \tag{21}$$

By combining (15) and (21), the correction factor (1 - k) becomes:

$$(1 - K) = \left[1 - \frac{N_0 (10^{-6}) \left[1 - e^{-\gamma (H_A - H_s)} \right]}{\gamma (H_A - H_s)} \right] \tag{22}$$

and

$$\cos \alpha' = \cos \alpha \, (1 - K) \tag{23}$$

$$\cos \beta' = \cos \beta \, (1 - K) \tag{24}$$

$\cos \alpha$ and $\cos \beta$ being direction cosines to a star coincident with the flashing light and $\cos \alpha'$, $\cos \beta'$ direction cosines to the aircraft.

Equation 22 is what is currently employed in the calibration calculation at the Physical Science Laboratory, New Mexico State University.

The next section will show that the expected radio phase meter readings $\Delta\varphi_\alpha$ and $\Delta\varphi_\beta$ are given by:

$$\Delta\varphi_\alpha = [b \cos \alpha \, (1 - K) \, \bar{n}] \left[\frac{2\pi}{\lambda_0} \right] \text{ radians} \tag{25}$$

and

$$\Delta\varphi_\beta = [b \cos \beta \, (1 - K) \, \bar{n}] \left[\frac{2\pi}{\lambda_0} \right] \text{ radians} \tag{26}$$

where:

b = baseline length, $\cos \alpha$, $\cos \beta$ are direction cosines corresponding to line-of-sight to star occulated by flashing light

$(1 - K)$ = correction factor to obtain line-of-sight to aircraft

$$\bar{n} = \frac{1}{H_A - H_s} \int_{H_s}^{H_A} n(h)\, dh = \text{average radio index of refraction between tracking station and aircraft altitudes}$$

λ_0 = free-space wavelength of received frequency

5.2 CALIBRATION AND RADIO REFRACTION

During the aircraft calibration flyby at a given site, radio phase data is recorded and the difference between the observed phase data and that "expected" is sent to the Goddard Space Flight Center as a correction to be applied to subsequent raw Minitrack phase data. During this calibration the "expected" Minitrack radio phase measurement is based upon the precise line of sight to aircraft adjusted for prevailing radio refraction conditions. The previous section discussed the conversion of star line-of-sight to aircraft line-of-sight. This section will now derive the radio refraction correction factor.

During calibration the ionosphere plays no part since the aircraft is necessarily well below the ionosphere's 85 km lower altitude limit. A most important point is that the radio phase readings measured during calibration are compared with precise line of sight data altered slightly to take into account the tropospheric radio refraction. The calibration is not a means for later adjusting raw spacecraft tracking data to either angle of arrival or line of sight measurements. The calibration accounts for on site biases associated with the Minitrack antenna system and electronics and does not provide a refraction correction for subsequent raw data recordings.

In order to calculate what the interferometer should read for a given line of sight geometry it is necessary to calculate the electrical path difference corresponding to the geometric path difference $S_1 - S_2$ (Figure 9). It will be shown that, for the aircraft geometry, the corresponding electrical path length is given by $\bar{n}(S_1 - S_2)$, where $\bar{n}$ is the average radio index of refraction between tracking site and aircraft altitudes.

With reference to Figure 9, in the absence of an atmosphere, the free space interferometer phase measurement would be given by:

$$\Delta\phi_0 = \frac{2\pi(S_1 - S_2)}{\lambda_0} \text{ (radians)} \qquad (27)$$

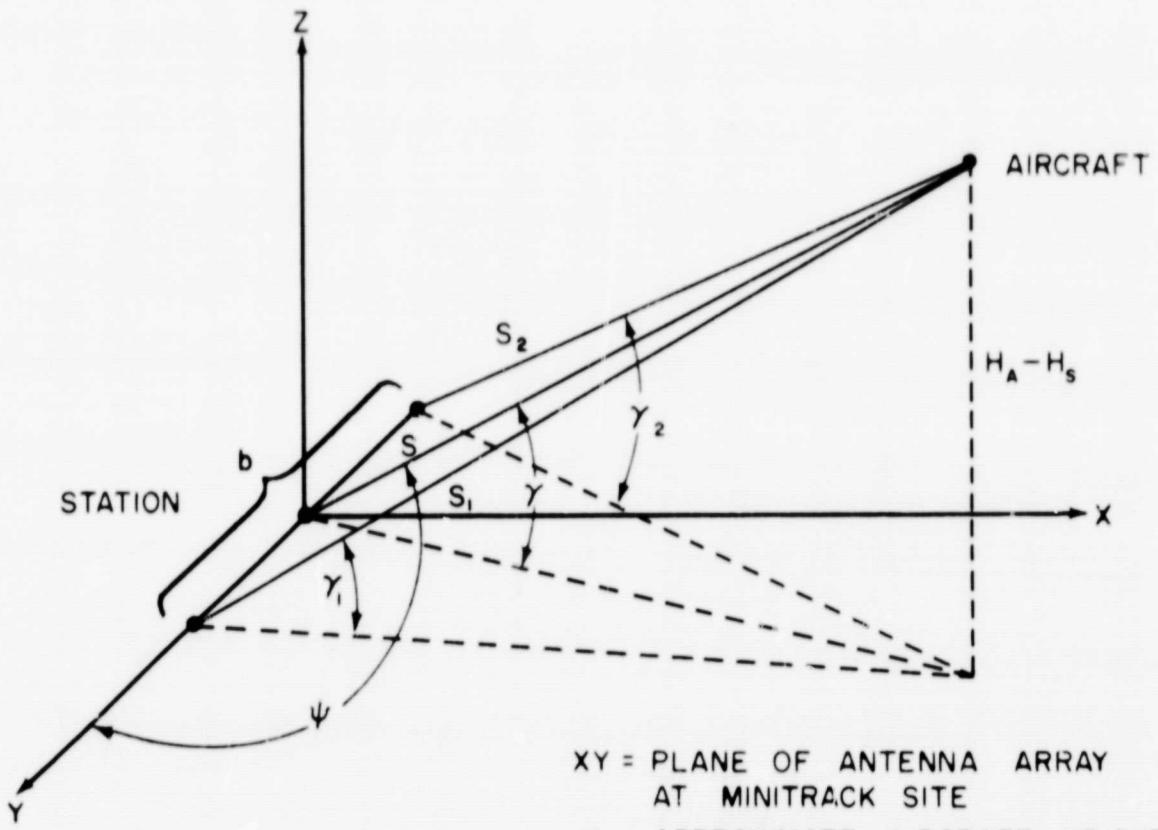

XY = PLANE OF ANTENNA ARRAY AT MINITRACK SITE

H_A = APPROXIMATE AIRCRAFT HEIGHT (NEGLECTING EARTH CURVATURE)

H_S = STATION ALTITUDE

NASA GSFC T&DS
MISSION & TRAJECTORY ANALYSIS DIVISION
BRANCH 551 DATE 2 Oct. 1969
BY P. Schmid PLOT NO. 1239

Figure 9–Aircraft Calibration Geometry

where

S_1 = geometric distance from phase center of antenna at one end of baseline to aircraft

S_2 = geometric distance from phase center of antenna at other end of baseline to aircraft

λ_0 = free space wavelength = c/f_0 and c is the speed of light in vacuum, the frequency of the received radio energy.

The frequency, f_0, will differ from the transmitted frequency by the one-way Doppler shift f_0 $(\dot{r}/c)$ where $\dot{r}$ is the radial velocity of the transmit beacon relative to the station. At 136 MHz this is entirely negligible relative to the expected uncertainty in measured surface index of refraction of ±1 N unit, that is, the ratio of ΔN (±1) to N_s (~ 300) is always large compared to $\dot{r}$ /c . The physics linking surface refractivity to wet and dry bulb temperature measurements and statements of expected accuracy are covered in detail in Reference 7.

Again with reference to Figure 9 the actual interferometer phase readings are given by:

$$\Delta\varphi = \frac{2\pi}{\lambda_0}\left[\int n(s)\,dS_1 - \int n(s)\,dS_2\right] \text{ radians} \qquad (28)$$

As pointed out by Bean and Thayer of NBS (Reference 16), equation (28) can be integrated assuming flat-earth conditions for elevation angles $E_0 > 10°$, slant range $r << a_0 \sin E_0$ (a_0 = earth radius), and for baselines of a few hundred meters or less.

These conditions are applicable to the aircraft flyby and hence, again with reference to Figure 9, equation (28) can be written as:

$$\Delta\varphi = \frac{2\pi}{\lambda_0 \sin\gamma_1}\int_{H_s}^{H_A} n(h)\,dh - \frac{2\pi}{\lambda_0 \sin\gamma_2}\int_{H_s}^{H_A} n(h)\,dh \text{ (radians)} \qquad (29)$$

and by the law of sines

$$\frac{S}{\sin\gamma_1} = \frac{S_1}{\sin\gamma}; \quad \frac{S}{\sin\gamma_2} = \frac{S_2}{\sin\gamma}$$

equation (29) becomes

$$\Delta\varphi = \frac{2\pi(S_1 - S_2)}{\lambda_0}\left(\frac{1}{H_A - H_s}\right)\int_{H_s}^{H_A} n(h)\,dh = \frac{2\pi(S_1 - S_2)}{\lambda_0}\bar{n} \text{ (radians)} \qquad (30)$$

With reference to figure 9, $S_1 - S_2$, at aircraft slant ranges, is given by:

$$S_1 - S_2 = b \cos \psi$$

for one Minitrack baseline $\psi \equiv \alpha'$, for the other orthogonal Minitrack baseline $\psi \equiv \beta'$ and relating these to the star direction cosines, α and β, equation (30) can be written as

$$\Delta\varphi_\alpha = [b \cos \alpha \, (1 - K) \, \bar{n}] \frac{2\pi}{\lambda_0} \text{ (radians)}$$

$$\Delta\varphi_\beta = [b \cos \beta \, (1 - K) \, \bar{n}] \frac{2\pi}{\lambda_0} \text{ (radians)} \qquad (31)$$

where the factor (1-k) was defined previously by equation (22).

In equation (31) $\Delta\varphi_\alpha$ and $\Delta\varphi_\beta$ represent the expected Minitrack phase readings during the aircraft flyby when the flashing light appears coincident with a star whose line-of-sight direction cosines are cos α and cos β respectively.

The average radio index $\bar{n}$ is calculated using the NBS exponential profile $n(h) = 1 + N_s \, (10^{-6}) \, e^{-kh}$. This profile when integrated and averaged results in:

$$\bar{n} = \frac{1 + N_s \, (10^{-6}) \, (1 - e^{-k(H_A - H_s)})}{k(H_A - H_s)} \qquad (32)$$

the decay factor, k, is calculated with an empirical relation formulated by NBS based upon a fit to 888 sets of data (Reference 14).

$$k = \log_e \frac{N_s}{N_s + \Delta N}$$

where ΔN represents the change in refractivity in the vertical direction 1 km above the tracking station.

$$\Delta N = -7.32\, e^{0.005577 N_s} \text{ (Reference 14)} \qquad (33)$$

Finally the surface refractivity is calculated from surface meteorological measurements using the relation:

$$N_s = \left(\frac{77.6}{T}\right)\left(P + \frac{4810\epsilon\,(RH)}{T}\right) \qquad (34)$$

where $n_s = 1 + N_s\,(10^{-6})$ surface radio index of refraction and

T = air temperature (°K)

P = total air pressure (millibars)

ϵ = saturation vapor pressure (millibars)

RH = relative humidity (Reference 21)

The optical refractivity, N_0, as previously indicated by equation (16) is equation (34) without the water vapor term.

Equations (31) through (34) are used by New Mexico State University in their reduction of Minitrack aircraft calibration data for the Goddard Space Flight Center.

5.3 ANGLE OF ARRIVAL CORRECTION EQUATIONS

As a matter of interest, the foregoing principles can now be applied to derive the flat earth approximation for the angular difference between elevation angle of arrival and line-of-sight for both optical and radio refraction. The only difference between the optical and radio cases is that $\bar{n}$ for the radio refraction includes the effect of water vapor within the earth's atmosphere.

For an interferometer such as Minitrack which has intersecting orthogonal baselines running East-West and North-South the phase readings are, as shown previously, given by:

$$\Delta\varphi_\alpha = \frac{2\pi b \cos E}{\lambda_0} \bar{n} \sin A$$

and

$$\Delta\varphi_\beta = \frac{2\pi b \cos E}{\lambda_0} \bar{n} \cos A \qquad (35)$$

Here, E, represents the line-of-sight elevation angle to the source and, A, the azimuth angle. But the phase measurement is also represented by the phase delay in terms of the number of wavelengths of delay within the media surrounding the antenna. The effective wavelength within the media in the vicinity of the antenna is λ_0 / n_s . In terms of the elevation angle of arrival, E_0, the following equations can thus be written:

$$\Delta\varphi_\alpha = \frac{2\pi b \cos E_0}{\lambda_0 / n_s} \sin A$$

$$\Delta\varphi_\beta = \frac{2\pi b \cos E_0}{\lambda_0 / n_s} \cos A \qquad (36)$$

Combining (35) and (36)

$$\bar{n} \cos E = n_s \cos E_0 \qquad (37)$$

This equation links elevation angle of arrival, E_0, to line-of-sight angle, E. But $E_0 = E + \Delta E$, where ΔE is a small perturbation and (37) can be expanded to obtain the approximation:

$$\Delta E \doteq \left(1 - \frac{\bar{n}}{n_s}\right) \cot E \tag{38}$$

Here ΔE is the elevation angle-of-arrival error due to the atmosphere. This result was also derived by R. H. Paul (equation 19 of Reference 16) using a somewhat different approach. Equation (38) can also be written in terms of refractivity, N, since:

$$\bar{n} = 1 + \bar{N}\,(10^{-6})$$

and

$$n_s = 1 + N_s\,(10^{-6})$$

In all cases the deviation from unity is 10^{-3} or less thus equation (38) can be written as

$$\Delta E = (N_s - \bar{N}) \cot E\,(10^{-6}) \tag{39}$$

Where as before, N_s, represents the radio surface refractivity varying from 200 to 400 depending upon geographical location and local meteorological conditions and $\bar{N}$ is the average refractivity between the station altitude and the altitude of the signal source. If the source is a spacecraft than $\bar{N}$ includes the effect of the ionosphere where the absolute sign of the refractivity term is negative (Reference 6). Equation (39) thus also indicates how the presence of the ionosphere increases the total ray bending as suggested previously by Figure 5. As the altitude of the spacecraft increases much above 5000 km, or for all spacecraft operating at 2 GHz or higher such that the ionosphere is no longer a significant influence, $\bar{N}$ tends to zero and equation (39) reduces to:

$$\Delta E \doteq N_s\,(10^{-6})\cot E$$

and to a first order:

$$\cot E = \cot E_0$$

or

$$\Delta E \doteq N_s\,(10^{-6})\cot E_0 \quad \text{(radians)} \tag{40}$$

This result, presented earlier as equation (2), is the usual tropospheric bending correction applied to elevation angle spacecraft tracking data for elevation angles above 10°. The same result is used for optical correction to star-light angle of arrival except N_0, the optical surface refractivity, is used instead of N_s, the radio-surface refractivity.

Finally, equations (38) and (40) can be used to derive equation (14) presented earlier for the angular difference, ϵ, between the line-of-sight to a star coincident with a flashing light on the Minitrack calibration aircraft and the line-of-sight to the aircraft.

With reference to Figure 8, the angle, ϵ, is the difference between the total star-light bending, $N_0(10^{-6})\cot E$, and the bending of the flashing light ray path relative to the line-of-sight to the aircraft, $(1 - \bar{n}/n_0)\cot E$ or

$$\epsilon = \left[(n_0 - 1) - \left(1 - \frac{\bar{n}}{n_0}\right)\right]\cot E$$

or (41)

$$\epsilon = \left(n_0 - 2 + \frac{\bar{n}}{n_0}\right)\cot E \quad \text{(radians)}$$

Equation (41) was presented earlier as equation (14) and presents a good approximation of elevation angle distortion for elevation angle, E_0, greater than 10° and slant ranges to the spacecraft much less than $a_0 \sin E_0$, where a_0 is the earth radius.

6.0 EFFECT OF IONOSPHERE ON MINITRACK MEASUREMENT

The elevation angle bias present in Minitrack measurements below elevation angles of 40° can be largely attributed to residual error after nominal ionospheric corrections have been applied. Unlike the troposphere, the ionosphere is much less predictable and as mentioned previously, ionospheric refraction effects vary inversely as the square of the radio frequency. One of the major sources of ionospheric modeling error has to do with the fact that the radio signal often traverses portions of the ionosphere several thousand kilometers from the tracking site, a situation where the usual spherically stratified Chapman model does not strictly apply. One means of minimizing the ionospheric refraction error is to use only data where the signal is traversing local night regions. Recent studies, however, indicate ionospheric propagation anomalies peaking at local midnight at the South American Minitrack sites (Santiago, Lima, and Quito) (Reference 22). These equatorial region anomalies appear to predominate in the East-West baseline which, as stated in Reference 22 is consistent with existing theories of ion plasma density alignment North to South along the Earth's magnetic field lines. Study of the phenomena and the effect on NASA 136 MHz telemetry, tracking and command signals is continuing (References 23 and 24).

6.1 THE INTERFEROMETER REFRACTION ERROR EQUATION

The inherent tropospheric correction to interferometer data was discussed in section 4.0. It was shown that the elevation angle calculated is given by:

$$E' = E_0 - N_s(10^{-6}) \cot E_0$$

$$E' \doteq E_0 - N_s(10^{-6}) \cot E \qquad (42)$$

for $E_0 > 10°$ where:

E_0 = elevation angle of arrival

E' = interferometer calculated angle

E = line-of-sight elevation angle

It was also shown in section 5.3 (equation 38) that the line-of-sight elevation angle, E, is linked to angle of arrival elevation, E_0, by:

$$E \doteq E_0 - \left(1 - \frac{\bar{n}}{n_s} \cot E\right) \tag{43}$$

Thus the total interferometer error is found by combining (42) and (43) to obtain:

$$\text{Interferometer Error} = E' - E \doteq -\bar{N}(10^{-6}) \cot E \tag{44}$$

which corresponds to Bean and Thayer's equation 26 in Reference 16. Equation (44) is a good approximation for $E > 10°$, interferometer baselines of a few hundred meters or less (such as Minitrack), and slant range to spacecraft, $r << a_0 \sin E$, where a_0 is the earth radius. Equation (44) is useful in qualitatively describing the effect of the ionosphere on Minitrack data when the spacecraft is within the ionosphere (100 < altitude < 1000 km). At 136 MHz the contribution to $\bar{N}$ due to the troposphere is negligible compared to the ionospheric contribution. This can be shown as follows. According to equation (32) for altitudes significantly above the troposphere scale height (~7 km) the tropospheric average refractivity is given by

$$\bar{N}_t = \frac{N_s(10^{-6})}{kH} \tag{45}$$

where:

H = spacecraft height above the tracking station

k = decay factor in exponential model, 1/k = 7 km.

For H = 200 km, $\bar{N}_t \doteq 12$ which is small when compared to the ionospheric contribution.

The ionospheric refractivity is given by:

$$N(h) = \frac{-40.3\, N_e(h)}{f^2} (10^6) \text{ (Reference 6)} \qquad (46)$$

where:

N_e = electron density (electrons/meter^3)

f = frequency (Hz)

For a daytime peak density at the height of maximum ionization, N_e takes on values of typically 0.5 (10^{12}) electrons/meter^3 and at 136 MHz this corresponds to a maximum ionospheric refractivity on the order of -2000. This value will taper off by a factor of 10 at the lower edge of the ionosphere (H = 85 km). However, the average contribution will be significantly greater than the tropospheric contribution $\overline{N}_t = 12$. An interesting observation is that, again by equation 44, and noting that the average refractivity due to the ionosphere is negative, the ray bending will be in the same direction as that due to the troposphere. With the interferometer, of course, the tropospheric bending is already inherently corrected for by the usual angle calculation discussed previously in section 4.0.

The "flat-earth" model (equation 44) is useful for qualitative ionospheric refraction discussion only since the range of validity includes the constraint $r << a_0 \sin E$. However a more satisfactory equation which includes Earth curvature has been presented by Bean and Thayer of the National Bureau of Standards where the interferometer error is given by:

$$\text{Interferometer Error} = \left[-10^{-6} \cot E \int_0^H N(h)\, dh \right] \left[\frac{1}{r \sin E} + \frac{1}{a_0 \sin^2 E} \right] \qquad (47)$$

$E > 10°$

$r >> b \quad b < 50$ km

where:

E = line-of-sight elevation angle

N(h) = vertical refractivity profile including both troposphere and ionosphere

r = slant range station to spacecraft

H = altitude of spacecraft above station

a_0 = earth radius

b = interferometer baseline (b = 120 meters for Minitrack).

For the "flat earth" approximation r sin E $\doteq$ H and r << a_0 sin E, equation (47) reduces to $-\bar{N}(10^{-6})$ cot E, presented previously as equation (44).

Equation 47 can be derived from Snell's law for a spherically stratified media. The result can also be obtained by ray tracing, through the atmosphere (again using Snell's law) to determine the difference between angle of arrival and line-of-sight. This can then be linked to the interferometer error by subtracting out the first order tropospheric correction of N_s (10^{-6}) cot E.

6.2 MINITRACK IONOSPHERIC REFRACTION

This section presents the Minitrack bias error which can be expected if ionospheric effects are neglected. A nominal correction based upon National Bureau of Standards (NBS) Monthly worldwide peak electron density predictions and some mathematical distribution model (such as a Chapman profile) often reduces the error by only 50%. As will be discussed shortly the greatest uncertainty is related to the F_2 layer vertical sounding (i.e. "zero") Maximum Usable Frequency (MUF). The peak electron density and hence refractivity is proportional to the square of the F_2 (zero) MUF.

As indicated by Figure 5 and equation 47, the Minitrack refraction error is separable into tropospheric and ionospheric components. At frequencies such as 136 MHz, where ionospheric bending is appreciable the tropospheric contribution in equation 47 is generally negligible if elevation angles above 10° and spacecraft altitudes above 100 km are considered. During aircraft calibration the reverse is true and only the troposphere is a consideration. By ray tracing (Reference 25) through the ionosphere and troposphere separately and then comparing with a trace through ionosphere plus troposphere, the validity of superposition of bending has been

verified. The difference between total bending due to the troposphere alone and N_s (10^{-6}) cot E_0 comprises the tropospheric contribution to the error in equation 47. The ionospheric caused elevation error in equation 47 can be obtained directly from a ray trace through the ionosphere alone.

Table I is an example of the Minitrack refraction error magnitude associated with a track of the 2000 km altitude geodetic satellite (GEOS-A) which was launched on 6 November 1965. It should be emphasized that exact refraction values will vary from site to site and depend upon the time of day as well as time of year. For the table a peak ionospheric density of 0.8 (10^{12}) electrons/meter^3 was assumed for daytime and 10^{11} electrons/meter^3 for nighttime.

TABLE I

Minitrack Refraction Error
(No Corrections Applied)

Elevation Angle (Degrees)	Tropospheric Bias (mr)	Ionospheric Bias (mr)	
		Day	Night
10	-0.06	2.25	0.30
15	-0.02	1.65	0.20
20	-0.01	1.25	0.15
30	-0.005	0.80	0.10
40	-0.002	0.50	0.05
60	-0.001	0.25	0.00
80	~-0.0005	0.10	0.00

Satellite Altitude = 2000 km

In Table I the term "bias" refers to that value which must be subtracted from the measured elevation to obtain "true" elevation. The minus sign on the troposphere bias simply indicates the extent to which the inherent N_s (10^{-6}) cot E correction of the interferometer overcompensates for the tropospheric bending. Also the ionospheric refraction is a maximum for satellites at an altitude of approximately 500 km. For an altitude of 500 km the ionospheric error values of Table I will be increased by approximately 25% at 10°, 50% at 20° and 70% at 30°. The ionospheric bias tabulated in Table I is also plotted in Figure 10. The parameters used to obtain the results of Table I and Figure 10 via a ray trace are as follows:

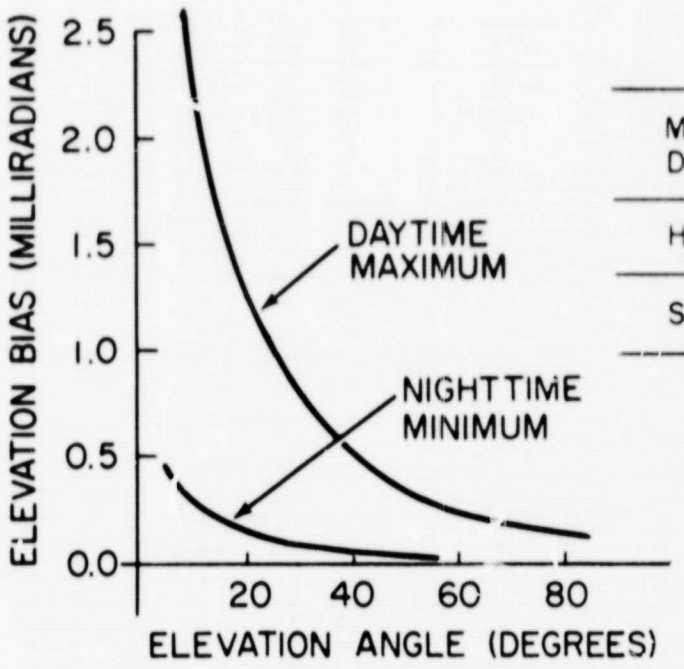

MINITRACK IONOSPHERIC PARAMETERS
(JANUARY 1966 PREDICTION)
REFERENCE 33

	DAY	NIGHT
MAXIMUM ELECTRON DENSITY (ELECTRONS/M^3)	$0.8(10^{12})$	$0.1(10^{12})$
HEIGHT OF MAXIMUM (KM)	300	250
SCALE HEIGHT (KM)	83	66

SATELLITE HEIGHT = 2000 KM

NASA GSFC T&DS
MISSION & TRAJECTORY ANALYSIS DIVISION
BRANCH 551 DATE 2 Oct. 1969
BY P. Schmid PLOT NO. 1240

Figure 10–Minitrack Elevation Angle of Arrival Bias Due to Ionosphere if no Correction Applied

TROPOSPHERE:

NBS exponential model

$$N(h) = N_s\, e^{-kh}$$

$$N_s = 350 \quad k = 0.16\ km^{-1}$$

$$n(h) = 1 + N(h)\ (10^{-6})$$

$$0 \leq h \leq 50\ km \qquad (48)$$

IONOSPHERE:

Chapman Model

$$N(h) = \frac{-40.3\, N_e(h)}{f^2}\, 10^6$$

$$f = 136 \text{ MHz}$$

$$n(h) = 1 + N(h)\, 10^{-6} \qquad h > 50 \text{ km}$$

$$N_e(h) = N_m\, e^{-1/2(1-Z-e^{-Z})} \quad \text{Reference 26} \tag{49}$$

N = maximum electron density = 0.8 (10^{12}) electron meter^3 representing nominal daytime value,

$Z = \frac{h - h_m}{H}$

h_m = 300 km representing a typical daytime height of maximum ionization

H = scale height = 83 km

h = 2000 km (GEOS-A altitude)

For a more precise determination of refraction effects all of the foregoing parameters must be estimated in view of particular station geographical locations, time of year, time of day, phase of sun spot cycle, prevailing meteorological conditions, and so on. It should be pointed out that at present, except for special tracking tests, only Minitrack data above elevation angles of 80° is used for orbit computation.

Figures 11 and 12 are plots of elevation angle residuals (observed elevation minus orbit calculated elevation) when no refraction corrections were applied to a 7 day stretch of GEOS-A Minitrack data (31 December 1965 to 6 January 1966). It is felt that the trended portion of these curves can be primarily attributed to refraction within the ionosphere.

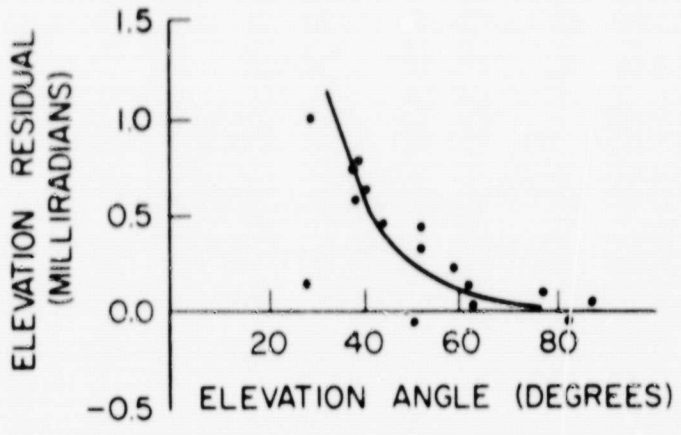

NEWFOUNDLAND
15H < t < 19H
LOCAL TIME

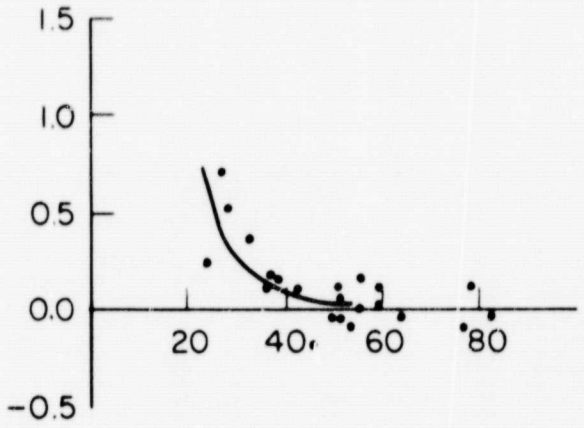

GRAND FORKS (NORTH DAKOTA)
15H < t < 19H
LOCAL TIME

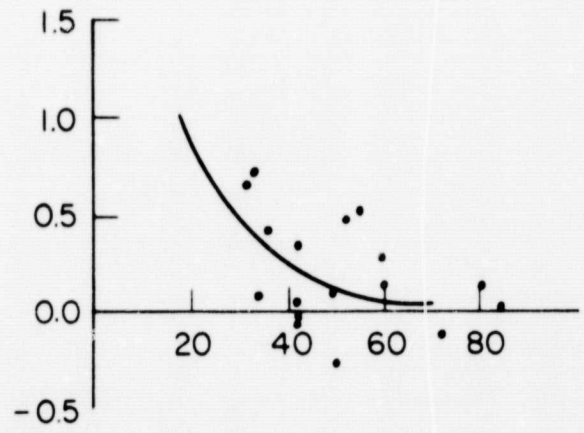

MOJAVE (CALIFORNIA)
15H < t < 19H
LOCAL TIME

Figure 11–Minitrack Elevation Angle Orbital Residuals
GEOS A (No Ionospheric Correction)

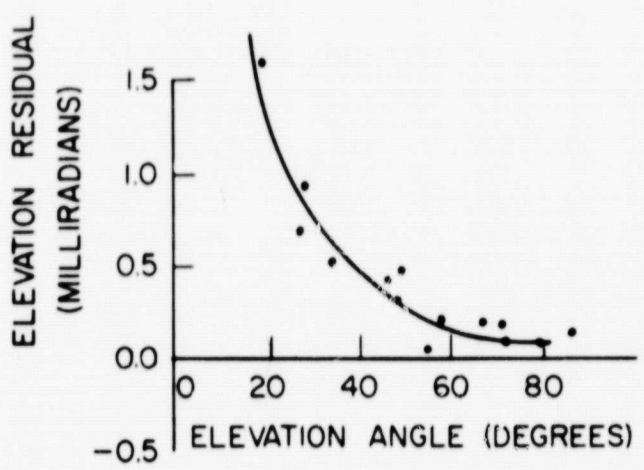

FORT MYERS (FLORIDA)
15H < t < 19H
LOCAL TIME

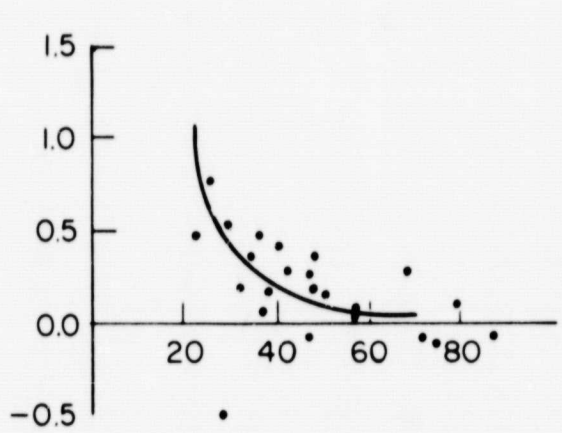

BLOSSOM POINT (MARYLAND)
15H < t < 19H
LOCAL TIME

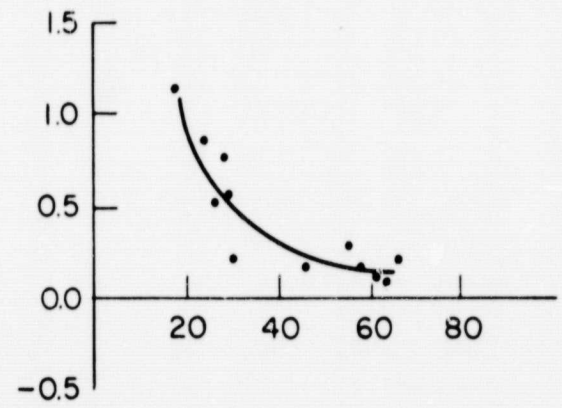

COLLEGE (ALASKA)
17H < t < 20H
LOCAL TIME

NASA GSFC T&DS
MISSION & TRAJECTORY ANALYSIS DIVISION
BRANCH 551 DATE 2 Oct. 1969
BY P. Schmid PLOT NO. 1242

Figure 12--Minitrack Elevation Angle Orbital Residuals
GEOS A (No Ionospheric Correction)

Finally, a most important point is that the tropospheric error indicated in Table I would be the only significant atmospheric refraction bias for an interferometer operating at frequencies above 2 GHz. For such a situation and for satellites where the slant range approaches the magnitude of the Earth radius multiplied by sin E, the interferometer refraction bias is given by the term associated with $1/a_0 \sin^2 E$ of equation 47. This is the expected interferometer refraction bias presented by the National Academy of Sciences (Reference 27) for interferometers with a baseline less than 3 km and operating at high enough frequencies such that the ionosphere is of no concern. The results in Reference 27 check those for the tropospheric refraction presented in Table I, the latter having been obtained from ray trace considerations.

One might wonder why 136 MHz is used instead of say 2GHz for the Minitrack frequency to eliminate ionospheric refraction. The primary reason is historical since in 1956, when Minitrack was first implemented, efficient S-Band spacecraft qualified hardware was not available. However the use of 136 MHz still has certain advantages over S-Band such as ease of signal acquisition and ambiguity resolution. That is, the transfer of radio energy from a spacecraft using a low gain antenna to a given ground effective antenna aperture is independent of operating frequency (Reference 28). However the respective beam and lobe widths vary inversely as the operating frequency. The antenna patterns corresponding to the Minitrack fine resolution array as presented in Reference 29 are given in Figure 13. Note that there are two such arrays for each of two orthogonal baselines. The complete Minitrack antenna layout as given in Reference 30 is shown in Figure 14.

6.3 IONOSPHERE MODEL PARAMETERS

The Chapman model presented in section 6.2 as equation 49 requires three input parameters - namely, the maximum electron density, N_m, the height of the maximum, h_m, and the scale height, H. Of these three the most critical parameters is the maximum density. The scale height has been formulated in terms of h_m (Reference 31).

$$H = 1.66\ [30 + 0.2\ (h_m - 200)] \tag{50}$$

where H and h_m are in km.

The height of the maximum, if no other information is available, can be taken as $h_m = 300$ km for daytime and $h_m = 250$ km for nighttime (Reference 32). The overall refraction is not a critical function of h_m and H.

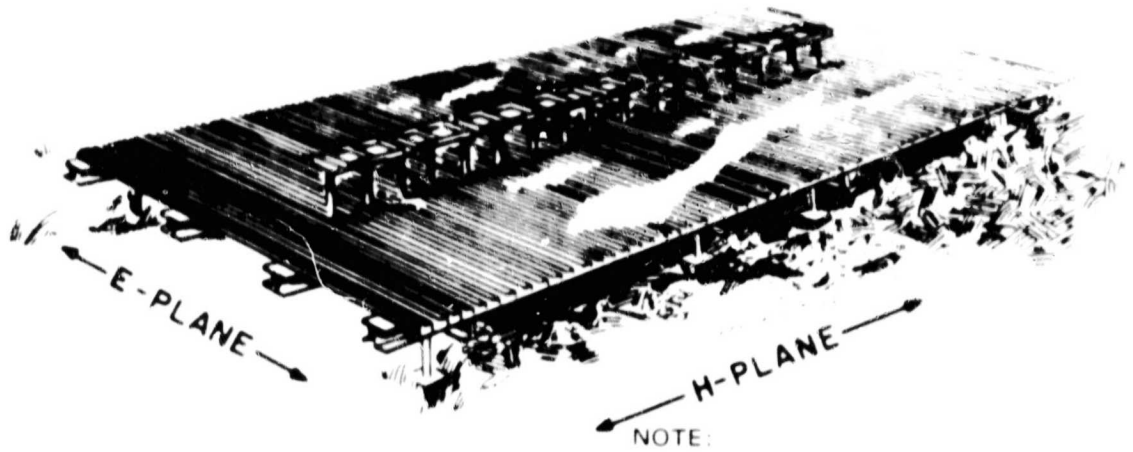

NOTE:
GAIN: 16.3 db ABOVE AN ISOTROPIC SOURCE
2 ARRAYS PER BASELINE

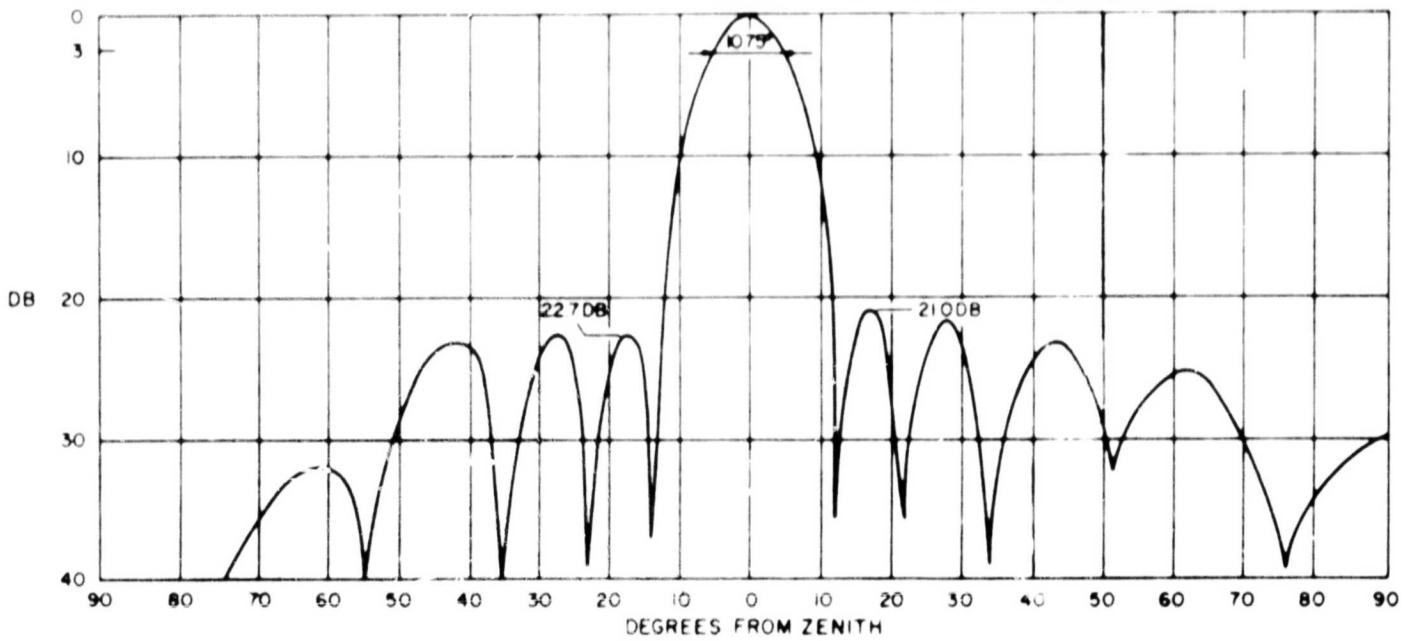

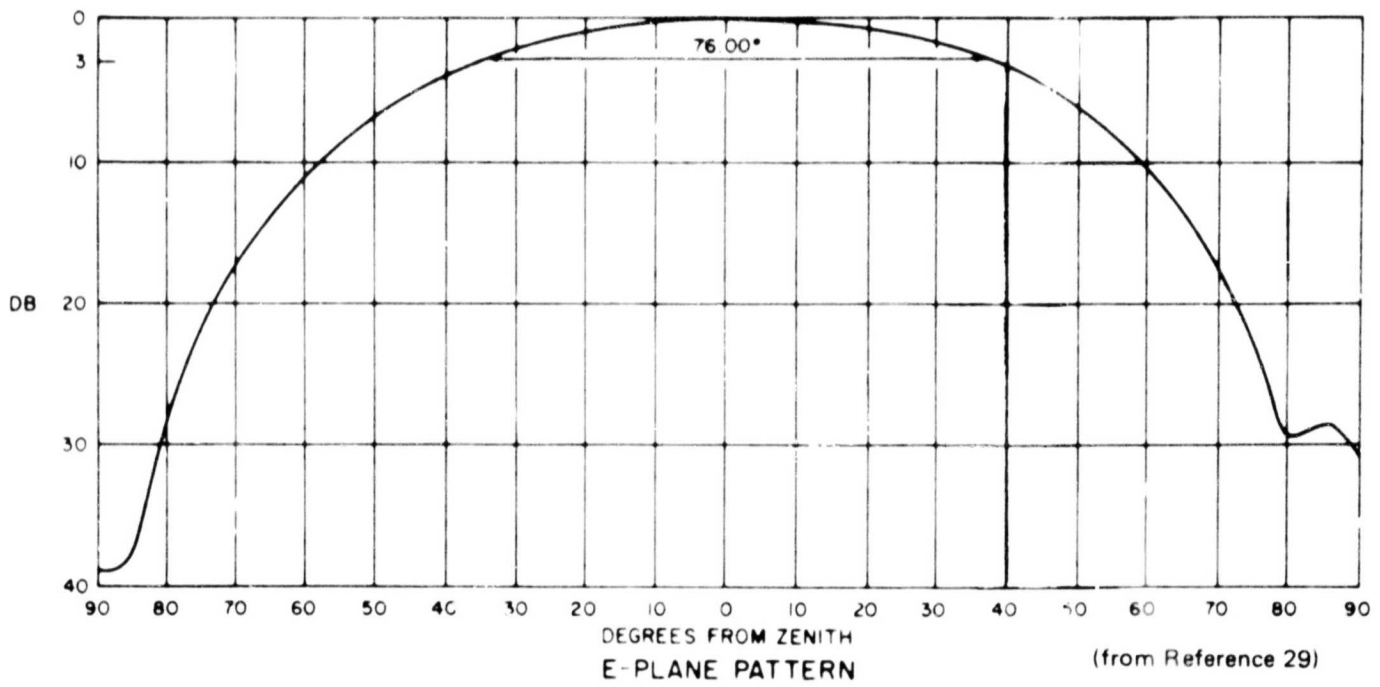

(from Reference 29)

Figure 13–136 MHz Minitrack Fine Antenna Array

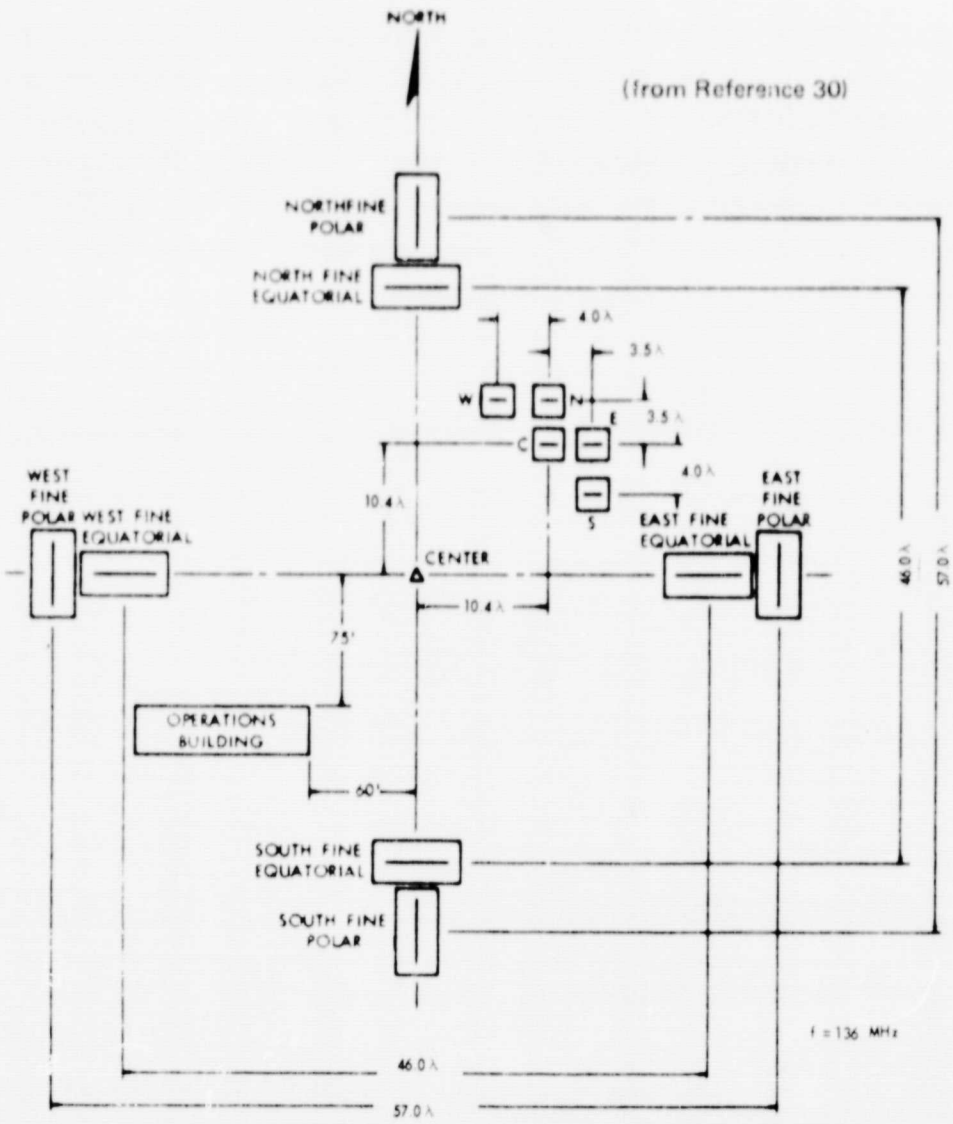

Figure 14–Relative Location and Function of Antennas in a Minitrack Antenna Field.

The following indicates a means for estimating the peak electron density of the ionosphere, utilizing the Institute for Telecommunication Sciences-Environmental Science Services Administration (formerly Central Radio Propagation Laboratory-NBS) monthly publication, "Ionospheric Predictions," in conjunction with a world-wide "gyro frequency" chart.

The publication, "Ionospheric Predictions" presents F_2 (zero) MUF (maximum usable frequency) world-wide charts (reference 33) for 3 months in advance. The charts present monthly mean values in 2-hour increments since the ionization variations are primarily diurnal during any given month. The "zero" in F_2 (zero) refers to zero ground "skip distance," i.e. vertical incidence ionosphere sounding. It can be shown (see for example, Reference 34) that for vertical incidence the critical frequency (highest frequency signal which will be returned to earth) is a function only of peak electron density and magnitude of the earth's magnetic field in the region of reflection. The direction of the earth's magnetic field does not influence the vertical "critical frequency." Because of the

presence of the earth's magnetic field, 3 discrete critical frequencies exist - namely, the ordinary critical frequency (this frequency would be the only critical frequency in the absence of the earth's magnetic field) and 2 so-called "extra-ordinary" critical frequencies. The F_2 (zero) MUF charts are for the highest critical frequency or the upper extra-ordinary frequency. This upper frequency results in the more predominant reflection since signals at the lower frequencies encounter appreciable attenuation.

The peak electron density is obtained from the ordinary critical frequency as:

$$N_e = \frac{f_c^2}{80} \tag{51}$$

where:

f_c = ordinary critical frequency (Hz)

N_e = peak electron density (electron/meter^3)

The F_2 (zero) MUF chart is for the upper extra-ordinary frequency (e.g. Figure 15) and is related to the ordinary critical frequency as follows:

where
$$f_{x_1} = \left(\frac{f_h^2}{4} + f_c^2\right)^{1/2} + \frac{f_h}{2} \tag{52}$$

f_{x_1} = upper extra-ordinary critical frequency as obtained from F_2 (zero) MUF chart.

f_c = ordinary critical frequency required to calculate maximum N_e (Equation 51).

f_h = "gyro frequency" which couples the effect of the earth's magnetic field into the ionosphere index of refraction. (Figure 15)
$= \frac{17.6}{2\pi} |\vec{B}|$ MHz (Reference 34)

$\vec{B}$ = earth's magnetic field (Gauss)

Since $f_h^2/4 << f_c^2$ in most cases then:

$$f_{x_1} = f_c + \frac{f_h}{2}$$

or the ordinary critical frequency is simply:

$$f_c = f_{x_1} - \frac{f_h}{2} \tag{53}$$

The predicted and observed F_2 (zero) MUF values seldom differ by more than 1 or 2 MHz with the larger differences occurring at the beginning or ending of a given month. Unfortunately the maximum electron density varies as the square of the critical frequency (Equation 51) so for a value of $f_c = 5$ MHz under worst case conditions (error of 2 MHz) the electron density could be off by a factor of 2. If the predicted critical frequency is off by only 1 MC then the maximum electron density in this case would be correct to within 30%. During midmonth, the F_2 (zero) MUF predicted values are accurate to within 80 to 90%.

The maximum electron density is given by:

$$N_M = \frac{\left(f_{x_1} - \frac{f_h}{2}\right)^2}{80} \text{ electrons/meter}^3 \tag{54}$$

f_{x_1} = frequency for appropriate geographical location, month, and time of day as obtained from an F_2 (zero) MUF chart such as Figure 15.

f_h = gyro frequency appropriate to a particular tracking site (Figure 16). Note that the gyro frequency is not a function of time.

N_m = estimated maximum electron density in the region above a particular tracking station (electrons/meter^3).

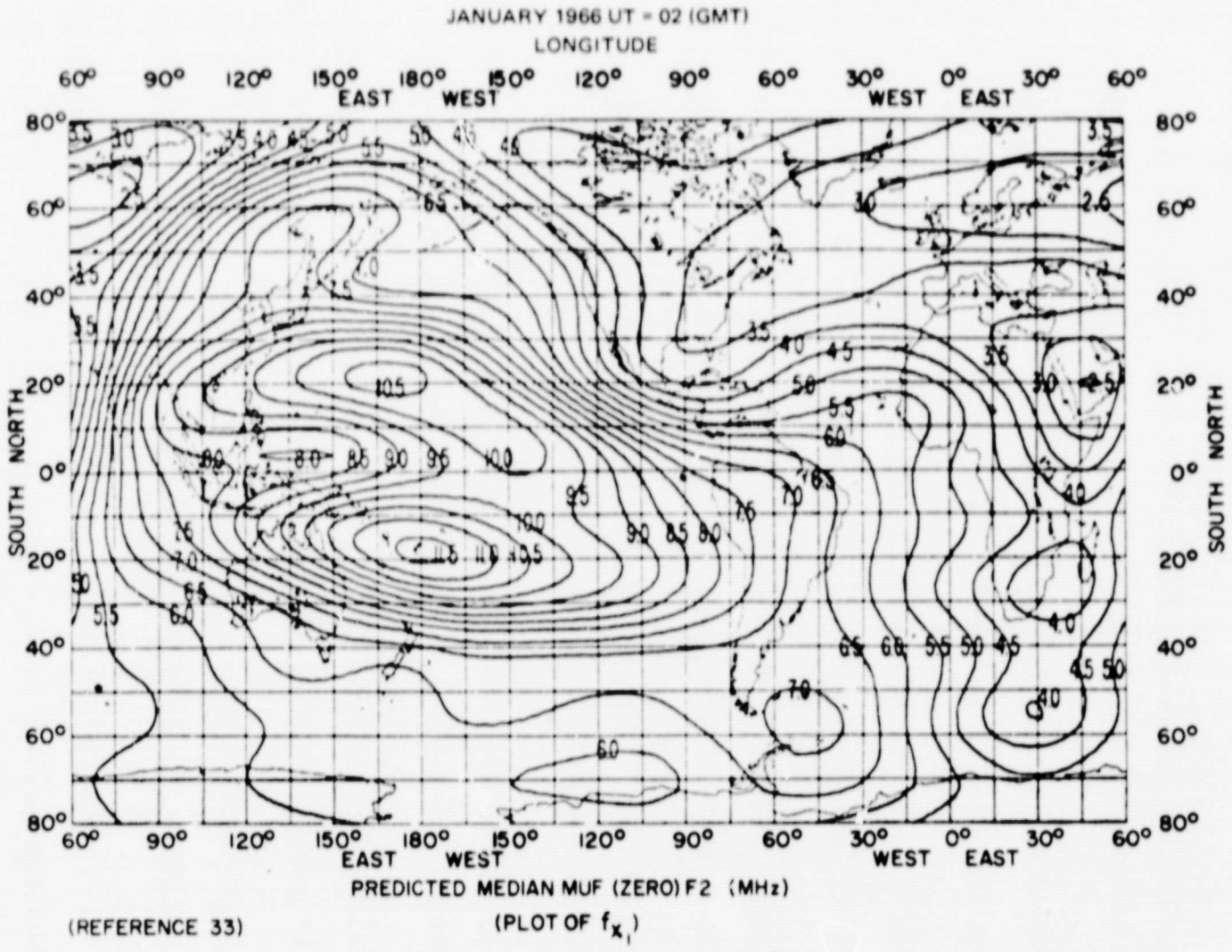

Figure 15–Example of F_2 (Zero) MUF Prediction (Reference 33)

The maximum electron density, N_M calculated by equation 53 is used in the Chapman model (equation 49) as a scale factor for the vertical electron density profile. To obtain best results the profile should be calculated for the region where the radio energy intercepts the region of maximum density. Generally, however, only the region above the tracking site is considered and spherical symmetry is assumed. The error thus introduced depends on satellite altitude and the relative steepness of contours such as given by Figure 15.

7.0 CONCLUSIONS

The atmosphere, for purposes of radiowave propagation, can be separated into two parts - namely, the troposphere (sea level to 30 km) and the ionosphere (85 km to 1000 km). Troposphere refraction effects are frequency independent in the range 100 MHz to 20,000 MHz. Ionospheric refraction is frequency

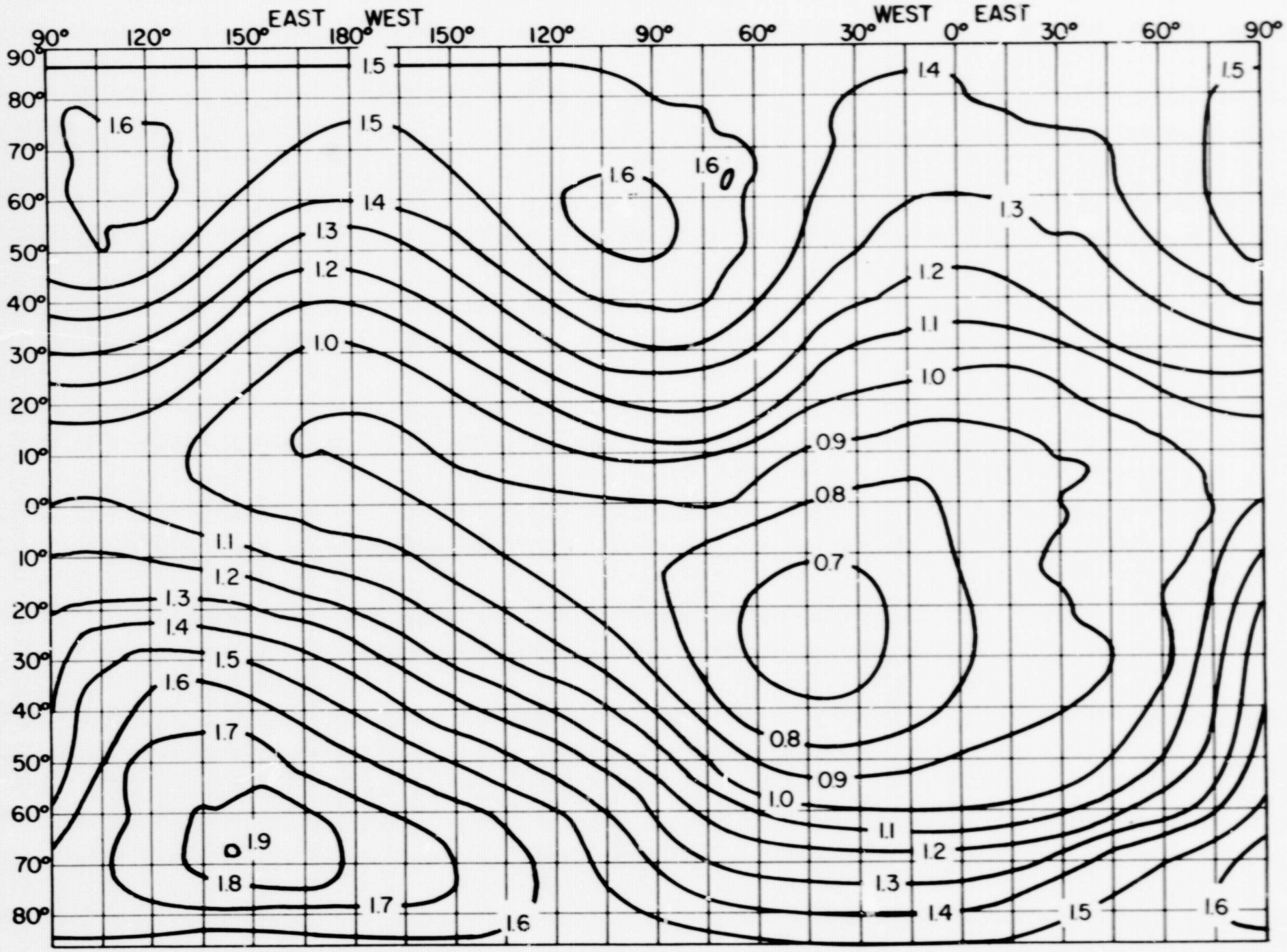

Figure 16--Gyro-Frequency Map of the World (Reference 35)

dependent varying inversely as the square of the operating frequency. At 136 MHz ionospheric refraction is significant. The atmosphere influences Minitrack measurements during aircraft calibration and during spacecraft tracking.

AIRCRAFT CALIBRATION

1. Only the troposphere is a consideration for both radio and optical (star background and flashing light) refraction.
2. The National Bureau of Standards exponential atmosphere coupled with "flat earth" geometry is satisfactory for modeling aircraft calibration refraction
3. For this model only the scalar quantity, surface refractivity, (optical and radio) is required.

SPACECRAFT TRACKING

1. Only the ionosphere is a consideration since the troposphere is corrected for inherently by the Minitrack calculation.
2. The Ionosphere can be modeled using a Chapman type profile to obtain estimates of ionospheric induced bias.
3. Recent top-side satellite soundings suggest an electron density decay with altitude somewhat less rapid than predicted by the Chapman model. An exponential decay in electron density above the height of maximum density appears to more closely approximate the true profile.
4. The parameters - Maximum electron density, height of maximum density, and scale height are required.
5. The extent to which corrections are successful is highly dependent on validity of estimates for maximum electron density.
6. Published prediction for maximum density used at the beginning and end of a given month can be such that as much as 50% of ionosphere residual bias remains after corrections are applied.

ACKNOWLEDGMENT

The cooperation of numerous personnel involved in Minitrack operations, data processing, and orbit computation is hereby gratefully acknowledged. This report was largely guided by the many clarifying discussions held with J. H. Berbert,

T. S. Golden, E. J. Lefferts, F. J. Lerch, J. W. Marini, J. D. Oosterhout, W. M. Rice, B. Rosenbaum, F. O. Vonbun, E. R. Watkins, Jr., (GSFC); H. C. Parker, R. F. Reich, (RCA); E. Good (New Mexico State University); and T. S. Englar (Mathematical Sciences Group).

REFERENCES

1. Marsh, J. G., C. E. Doll, R. J. Sandifer, and W. A. Taylor, "Intercomparison of the Minitrack and Optical Tracking Networks Using GEOS-1 Long Arc Orbital Solutions, Part 1," GSFC X-552-68-105, December 1967.

2. "Goddard Range and Range Rate System - Design Evaluation Report" R67-042 General Dynamics for the Goddard Space Flight Center, Greenbelt, Maryland, 13 December 1967.

3. Proceedings of the Apollo Unified S-Band Technical Conference NASA SP-87 Goddard Space Flight Center, July 14-15, 1965.

4. Barton, D. K., "Radar System Analysis" Prentice Hall, Englewood Cliffs, New Jersey, 1964.

5. "Applications Technological Satellite Range and Range Rate System - Design Evaluation Report" R-65-013 General Dynamics for the Goddard Space Flight Center, Greenbelt, Maryland, 1965.

6. Schmid, P. E., "Atmospheric Tracking Errors at S- and C-Band Frequencies," NASA TND-3470, August 1966.

7. Bean, B. R. and E. J. Dutton, "Radio Meteorology," NBS Monograph 92, 1 March 1966.

8. Goddard Directory of Tracking Station Locations, GSFC X-554-67-54 as updated through November 1968.

9. Oosterhout, J. D., Code 514 GSFC, "Minitrack Calibration," memorandum to C. H. Looney, Jr., Code 510, GSFC, August 19, 1968.

10. Martin, C. F., and J. R. Vetter, "Error Sensitivity Function Catalog," Wolf Research and Development Corporation, Riverdale, Maryland, for NASA Wallops Island, April 1969.

11. Mengel, J. T., "Tracking the Earth Satellite, and Data Transmission by Radio," Proc. IRE, June 1956.

12. Schroeder, C. A., C. H. Looney, Jr., and H. E. Carpenter, Jr., "Tracking Orbits of Man-Made Moons," Electronics, 2 January 1959.

13. Schmid, P. E., "The Conversion of Fundamental Tracking Data to Metric Form," GSFC X-551-69-3, January 1969.

14. Saxton, J. A., (Editor), "Advances in Radio Research," Volume 1, Academic Press, London-New York, 1964.

15. Barton, D. K., (Editor), "Report of AD HOC Panel on Electromagnetic Propagation" in National Academy of Sciences Final Report, Washington, National Academy of Sciences, February 1963.

16. Paul, R. H., G. D. Thayer and B. R. Bean, "A Comparison of Radar and Radio Interferometer Refraction Errors," IEEE Transactions on Aerospace and Electronic Systems, March 1969.

17. Habib, E. J., J. N. Bradford, J. H. Berbert, P. D. Engels, and J. D. Oosterhout, Minitrack System Training Manual, Part VI, Calibration of Minitrack, September 1958.

18. Good, E. W., J. H. Berbert, and J. D. Oosterhout, "Reduction of the Minitrack Astrographic Plates," Volume 6 Number 6, Photographic Science and Engineering, November-December, 1962.

19. Vonbun, F. O., "Correction for Atmospheric Refraction at the NASA Minitrack Stations," NASA TN D-1448, August 1962.

20. Bean, B. R. and G. D. Thayer, "CRPL Exponential Reference Atmosphere," NBS Monograph 4, 29 October 1959.

21. Bean, B. R., J. D. Horn and A. M. Ozanich, Jr., "Climatic Charts and Data of the Radio Refractive Index for the United States and the World," National Bureau of Standards Monograph 22, 25 November 1960.

22. Golden, T. S., "Ionospheric Distortion of Minitrack Signals in South America," GSFC X-525-68-56, February 1968.

23. Golden, T. S., "A Proposal for Measuring the Correlation Distance of Equatorial Ionospheric Disturbances," X-525-68-302, August 1968.

24. Golden, T. S., "Effects of Differential Signal Amplitudes in the Minitrack System," GSFC X-525-68-14, January 1968.

25. Rosenbaum, B. and N. Snow, "A Programmed Mathematical Model to Simulate the Bending of Radio Waves in Atmospheric Propagation," GSFC X-551-68-367, May 1968.

26. Kelso, John M., "Radio Ray Propagation in the Ionosphere," McGraw Hill Book Company, N.Y., 1964.

27. Barton, D. K., (Editor), "Report of the AD HOC Panel on Electromagnetic Propagation," National Academy of Sciences, National Research Council, Final Report, February 1963.

28. Schmid, P. E., "The Feasibility of a Direct Relay of Apollo Spacecraft Data via a Communication Satellite," NASA TN D-4048, August 1967.

29. Lantz, Paul A., and G. R. Thibodeau, "NASA Space Directed Antennas," GSFC X-525-67-430, September 1967.

30. Watkins, Jr., E. R., "Preprocessing of Minitrack Data," NASA TN D-5042, May, 1969.

31. Freeman, J. J., "Final Report on Ionospheric Correction to Tracking Parameters," Final Report Under NAS 509782, Goddard Space Flight Center, Greenbelt, Maryland, 3 November 1965.

32. Berger, W. J. and J. R. Ricupito, "Refraction Correction Studies," Aeronutronic Publication Number U-954, For U. S. Army Ballistic Missile Agency, Redstone Arsenal, Alabama Under Contract No. DA-04-495-506 ORD-1900, July 29, 1960.

33. Environmental Science Services Administration, "Ionospheric Predictions," annual subscription available from the Institute for Telecommunication Sciences-ESSA (formerly Central Radio Propagation Laboratory), published monthly with data 3 months in advance. January 1966, Number 34, issued October 1965.

34. Bremmer, H., "Terrestrial Radio Waves," Elsevier Publishing Company, Amsterdam - New York, p. 276-284, 1949.

35. Davies, K., "Ionospheric Radio Propagation," National Bureau of Standards Monograph 80, November 1965.